Combustion and Flame 238 (2022) 111867

Contents lists available at ScienceDirect

Combustion and Flame

journal homepage: www.elsevier.com/locate/combustflame

Comparison of methane combustion mechanisms using laminar burning velocity measurements

Peng Zhang [a], István Gyula Zsély [a,*], Máté Papp [a], Tibor Nagy [b], Tamás Turányi [a]

[a] Institute of Chemistry, ELTE Eötvös Loránd University, Budapest, Hungary
[b] Institute of Materials and Environmental Chemistry, Research Centre for Natural Sciences, Eötvös Loránd Research Network, Budapest, Hungary

ARTICLE INFO

Article history:
Received 26 July 2021
Revised 8 November 2021
Accepted 10 November 2021
Available online 6 December 2021

Keywords:
Methane combustion
Detailed mechanisms
Mechanism testing
Mechanism development

ABSTRACT

Large amount of experimental data for laminar burning velocity (LBV) measurements of methane (+ H_2/CO) – oxygen – diluent mixtures (5500 data points in 646 datasets) covering wide ranges of equivalence ratio, diluent ratio, cold side temperature and pressure were collected from 111 publications. The diluents included N_2, H_2O, CO_2, Ar and He. The data files are available on the ReSpecTh site (http://respecth.hu). Performances of 12 methane combustion mechanisms on reproducing these LBV measurements were analyzed according to experiment types and conditions. Most mechanisms could predict well the LBVs for stoichiometric and fuel-lean mixtures and for diluent ratios higher than 60%. The performances of several mechanisms were relatively poor at other conditions. Focusing on the operating conditions of natural gas engines, we recommend the application of mechanisms FFCM-I-2016, SanDiego-2014, and NUIG1.1-2021 for engine simulations. Mechanisms Aramco-II-2016, Konnov-2009, Caltech-2015 and Glarborg-2018 have the lowest average errors for the reproduction of all available methane LBV data. Using local sensitivity analysis on the most accurate mechanisms, we identified 29 important elementary reactions, which, however, were not present in all the 12 mechanisms. We also collected large amount of directly measured and theoretically calculated rate coefficients for these reactions and compared them with the rate coefficients used in the 12 mechanisms. Reactions found important in any of the Aramco-II-2016, Konnov-2009 and Glarborg-2018 mechanisms, but missing from the Aramco-II-2016, Konnov-2009, Glarborg-2018, Caltech-2015, FFCM-I-2016 and NUIG1.1-2021 mechanisms were added to these six mechanisms to investigate if the extended mechanism performs better than the original one. Some of the extended mechanisms became the best performing mechanisms.

1. Introduction

Widespread applications of renewable fuels have been seen in recent years. These fuels include H_2 produced by electrolysis of water using surplus electric energy, and NH_3 produced from H_2 and N_2. However, natural gas is still a very prospective fuel considering its huge reserves, safety and the convenience of its application. Also, utilization of renewable H_2 and NH_3 is frequently planned in the form of co-combustion with natural gas. The main component of natural gas is methane, therefore, understanding of the chemical kinetics of methane combustion is important for the development of combustor technologies. In our recent article [1] we reported the collection of large amount of methane ignition delay time measurements carried out in shock tubes and rapid compression machines, and testing 13 recent methane combustion mechanisms against these experimental data. Another fundamental measurable property of methane combustion is the laminar burning velocity (LBV). In this work, recent methane combustion mechanisms were tested using LBV experimental data.

Few works have investigated methane combustion mechanisms systematically using LBV measurements under wide condition ranges, although large amount of LBV experimental data are available for methane-containing mixtures. Konnov et al. [2] reviewed the LBV measurements for methane (and several other fuels) and evaluated the performance of San Diego mech (denoted here as SanDiego-2016) [3], USC mech II (USC-II-2007) [4], GRI mech 3.0 (GRI3.0-1999) [5] and Konnov mech 0.5 (Konnov-2009) [6] for methane/air mixtures under wide ranges of experimental data, which included cold side temperatures from 300 K to 443 K, pressures from 1 atm to 70 atm, equivalence ratios from 0.55 to 1.7 and

* Corresponding author.
E-mail address: zsigy@chem.elte.hu (I.G. Zsély).

https://doi.org/10.1016/j.combustflame.2021.111867

various diluent ratios. Mazas et al. [7] compared two mechanisms, GRI-mech 3.0 (GRI3.0-1999) [5] and the mechanism of Le Cong and Dagaut [8], under atmospheric pressure and in a cold side temperature range of 298 to 473 K, for $CH_4/O_2/N_2/H_2O$ mixtures. Varghese et al. [9] investigated the performance of GRI-Mech-3.0 (GRI3.0–1999) [5], Aramco-2 (Aramco-II-2016) [10] and FFCM-I (FFCM-I-2016) [11] on reproducing the LBVs of methane – air mixtures under wide ranges of conditions (cold side temperature 350–650 K, pressure 1 – 5 atm and equivalence ratio 0.6–1.4). Wang et al. [12] assessed GRI-3.0 (GRI3.0-1999) [5] and the high-pressure mechanism of Yang et al. [13,14] for $CH_4/O_2/N_2$ and oxygen-enriched $CH_4/O_2/CO_2$ mixtures at room cold side temperature (298 K) and high pressures (from 0.1 to 0.5 MPa). Nilsson et al. [15] analyzed the performance of Aramco-2.0 (Aramco-II-2016) [10] and a mechanism developed by Konnov et al. [16] on predicting the LBVs of CH_4–air mixture at cold side temperatures of 298–338 K, atmospheric pressure and equivalence ratios of 0.6–1.5. Wang et al. [17] recently compared measured laminar burning velocities with ones simulated by seven methane combustion mechanisms for a stoichiometric mixture with N_2 and He diluents, at typical temperature and pressure ranges of natural gas engines. They found that mechanism FFCM-1 (FFCM-I-2016) [11] reproduced the best their measurements.

Large number of LBV measurements of methane/oxygen/diluent mixtures have been carried out by many research groups. In several investigations H_2 and/or CO were added to the methane fuel. An extensive literature review was performed on the laminar burning velocities of such mixtures, and in total 646 datasets, comprising 5500 data points, were collected from 111 publications. To promote the elaboration and validation of combustion mechanisms, these data have to be systematically collected in a well-defined format. We have set up the ReSpecTh Information System [18], which stores thousands of combustion experimental data sets in an organized way in ReSpecTh Kinetics Data (RKD) format XML files [19]. These files include indirect combustion measurements, and also rate coefficient determinations by direct measurements and theoretical calculations.

For a systematic review of methane combustion mechanisms, we collected 646 sets of methane LBV experimental data in the literature and stored them in RKD format XML files. The experiments were simulated by 12 widely used combustion mechanisms and a quantitative assessment of their performance was given over a wide range of conditions from various aspects. Pairwise correlations between the prediction errors of the mechanisms were calculated to explore similarities between them. We also assessed the performance of the mechanisms specifically at the operating conditions of natural gas engines, which is a major engineering application of methane combustion. Local sensitivity analysis was carried out in order to identify important reactions, whose rate coefficients directly affect the performance of mechanisms in reproducing methane LBV measurements. Reaction steps were identified that were not present in some good mechanisms, but found to be important in the three best performing mechanisms. These missing reactions were added and it resulted in the improvement of several published mechanisms.

2. Methodology

Turányi et al. [20,21] suggested a systematic method for the assessment of the performance of combustion mechanisms. This approach has been used on the comparison of widely used mechanisms of several fuels, like hydrogen [21], synthesis gas [22], methanol [23], ethanol [24], ammonia [25] and methane [1]. The method utilizes two error functions, the mean squared error function (E) [20] and the mean signed deviation function (D) [21]. In both error functions, each deviation term between the simulated and measured data is normalized by the corresponding one standard deviation error of the experimental determination. While error function E quantifies the predicting power of a mechanism, the signed deviation D can tell whether a given mechanism systematically under- or over-predicts the experimental data on average. The two functions are defined as:

$$\delta_{ij} = \frac{Y_{\mathrm{sim},ij} - Y_{\mathrm{exp},ij}}{\sigma\left(Y_{\mathrm{exp},ij}\right)}$$

$$E = \frac{1}{N}\sum_{i=1}^{N}\frac{1}{N_i}\sum_{j=1}^{N_i}\delta_{ij}^2$$

$$D = \frac{1}{N}\sum_{i=1}^{N}\frac{1}{N_i}\sum_{j=1}^{N_i}\delta_{ij}$$

where

$$Y_{ij} = \begin{cases} y_{ij} & \text{if } \sigma\left(y_{\mathrm{exp},ij}\right) \approx \text{constant} \\ \ln y_{ij} & \text{if } \sigma\left(\ln y_{\mathrm{exp},ij}\right) \approx \text{constant} \end{cases}$$

In the equations above, i is the index of the data set, $y_{\mathrm{sim},ij}$ is the jth simulated data point, $y_{\mathrm{exp},ij}$ is the jth experimental data point, $\sigma\left(y_{\mathrm{exp},ij}\right)$ is the estimated standard deviation of the jth experimental data point and N_i is the number of data points in dataset i; N is the number of datasets. δ_{ij} denotes the standardized signed deviations. We considered that the LBV data can be better characterized by constant absolute error, based on the investigations of Olm et al. (see article [22], Supplementary, Appendix A). Thus, no transformation was applied to it ($Y_{ij} = y_{ij}$).

In this article we introduce σ_D, the standard deviation of the D value in order to assess the statistical confidence of systematic under- and overprediction indicated by value D.

$$\sigma_D = \sqrt{\frac{E - D^2}{\sum_{i=1}^{N} N_i - 1}}$$

If $D + 2\sigma_D < 0$ or $0 < D - 2\sigma_D$, then we can state with 95% statistical confidence that the mechanism systematically under- or overpredicts the experimental data, respectively. The derivation of the equation above is provided in Part 2 of Supplementary 1.

The Pearson correlation coefficient (C) characterizes the pairwise similarity between mechanisms a and b with respect to their simulation results [21]. These coefficients are defined as:

$$C^{ab} = \frac{1}{N}\sum_{i=1}^{N}\frac{\sum_{j=1}^{N_i}\left(D_{ij}^{a} - \bar{D}_i^{a}\right)\left(D_{ij}^{b} - \bar{D}_i^{b}\right)}{\sqrt{\sum_{j=1}^{N_i}\left(D_{ij}^{a} - \bar{D}_i^{a}\right)^2}\sqrt{\sum_{j=1}^{N_i}\left(D_{ij}^{b} - \bar{D}_i^{b}\right)^2}}$$

where

$$D_{ij}^{a} = Y_{\mathrm{sim},ij}^{a} - Y_{\mathrm{exp},ij}$$

$$\bar{D}_{ij}^{a} = \frac{1}{N_i}\sum_{j=1}^{N_i} D_{ij}^{a}$$

Analogous definitions were applied to quantities with superscript b. At the estimation of the standard deviation of the data points, we considered both uncertainty $\sigma_{\mathrm{exp},ij}$ provided by the experimentalist and the $\sigma_{\mathrm{stat},i}$statistical scatter of the data points:

$$\sigma_{ij} = \sqrt{\sigma_{\mathrm{stat},i}^2 + \sigma_{\mathrm{exp},ij}^2}$$

where

$$\sigma_{\mathrm{stat},i}^2 = \frac{\sum_{j=1}^{N_i}\left(Y_{\mathrm{exp},ij} - Y_{\mathrm{fit1},i}\left(x_{ij}\right)\right)^2}{N_{\mathrm{DOF},i}}$$

Table 1
Summary of the methane LBV experimental data sorted according to measurement types (CTF: counterflow twin-flame method, SJF: single jet flame, FCM: flame cone method, HFM: heat flux method, OPF: outwardly propagating flame method, HDC: externally heated diverging channel method). The table includes the numbers of datasets and data points, ranges for cold side temperature T, pressure p, equivalence ratio φ, and the combinations of fuels and diluents together with the number of corresponding data points.

Type	Sets	Points	T / K	p / atm	φ	Fuel types		Diluent types	
CTF	42	400	298–343	0.24–4.51	0.31–1.80	CH_4 (284) CH_4/CO (40)	CH_4/H_2 (56) CH_4/H_2/CO (20)	N_2 (334) Ar (13)	N_2/CO_2 (42) CO_2 (11)
SJF	13	92	295–298	1	0.48–1.56	CH_4 (71) CH_4/CO (8)	CH_4/H_2 (13)	N_2 (77)	N_2/CO_2 (15)
FCM	63	519	295–600	0.83–98.7	0.39–2.21	CH_4 (403) CH_4/H_2/CO (60)	CH_4/H_2 (56)	N_2 (302) CO_2 (45) N_2/He (22) No diluent (16)	N_2/H_2O (81) H_2O (31) N_2/CO_2 (22)
HFM	188	2045	293– 455	0.1–5.0	0.39–3.34	CH_4 (1145) CH_4/CO (119)	CH_4/H_2 (755) CH_4/H_2/CO (26)	N_2 (1703) N_2/CO_2 (111) Ar (38)	CO_2 (148) No diluent (45)
OPF	321	2267	290–718	0.06–72.8	0.10–4.50	CH_4 (1782) CH_4/H_2/CO (47)	CH_4/H_2 (438)	N_2 (1708) CO_2 (104) N_2/He (174) CO_2/He (17) $N_2/CO_2/H_2O$ (11)	N_2/CO_2 (177) He (39) N_2/Ar (26) N_2/H_2O (11)
HDC	19	177	300–700	1–5	0.60–1.41	CH_4 (147)	CH_4/H_2/CO (30)	N_2 (147)	N_2/CO_2 (30)

Here $Y_{\mathrm{fit1},i}(x_{ij})$ is the trendline value that corresponds to experimental point $Y_{\mathrm{exp},ij}$, x_{ij} is the systematically changed condition parameter within the dataset, $N_{\mathrm{DOF},i} = N_i - n_{\mathrm{fit1},i}$ is the number of degrees of freedom, and $n_{\mathrm{fit1},i}$ is the number of parameters in the fitting function. This trendline was obtained by spline or polynomial fitting using code Minimal Spline Fit [26]. The theoretical background of the determination of the trendline has been published in [27].

3. Collection of experimental data

The combustion characteristics of methane containing mixtures have been widely studied. In this work, we consider only those laminar burning velocity measurements in which the fuel mixtures contain methane and may also contain H_2 and/or CO, but no higher hydrocarbons or oxygenated species. Details of the conditions covered by the experimental datasets are given in Table A of the Supplementary Material. The measurements had been carried out by the following six experimental methods: counterflow twin-flame method (CTF) [28], single jet flame (SJF) [29,30], flame cone method (FCM) [31], heat flux method (HFM) [32], outwardly propagating flame method (OPF) [33,34] and externally heated diverging channel method (HDC) [35]. Egolfopoulos et al. [36] reviewed experimental methods CTF, OPF, HFM, and SJF. Recently, Konnov and coworkers [2] systematically reviewed all the above experimental methods.

An overview of the covered ranges of initial conditions, fuel and diluent types is given in Table 1, separately for each experimental method. Cold side temperatures and pressures, equivalence ratios, and diluent ratios vary in the range of 290–718 K, 0.06–98.7 atm, 0.1–4.5, and 0–0.8518, respectively. Diluent ratio is interpreted as the total molar ratio of the non-fuel and non-oxidizer components in the mixture. The ranges of initial conditions covered by the collected LBV measurements are summarized in Fig. 1, which presents the pairwise distributions of temperature, pressure, equivalence ratio, and diluent ratio for all collected experimental data points. Figure 1 shows that the distributions of conditions are rather uneven and exhibit certain patterns. For example, at high cold side temperatures the diluent ratios for most measurements are around 0.70–0.80.

Figure 1 also shows that the measurements based on different experimental methods belong to different areas of conditions. The SJF method was used for measurements at atmospheric pressure and room temperature only. The other experimental methods were used in wider ranges of conditions. CTF, HFM and HDC were used to measure the LBVs in the pressure range of 1 to 5 atm; the measured highest temperatures of CTF and HFM are 343 K and 455 K, respectively, while the highest temperature among the HDC measurements could reach 700 K. Furthermore, all the high pressure ($>$ 5 atm) measurements were carried out by OPF and FCM, and the cold side temperature in these measurements could be as high as 600 K.

Some papers provided experimental uncertainties that are characteristic for the whole dataset. In this case the estimated standard deviation $\sigma_{ij}$of the data points is identical for all points in the dataset. These standard deviations are given in column 4 of Table A in Supplementary 1. In other papers, the uncertainties of the points were given as a percentage of the measured flame velocity, resulting in different absolute error for each point in a dataset. In such cases, we assigned absolute standard deviations to each individual point after transforming the relative error. For these cases column 4 of Table A contains the range of standard deviations in the dataset and the actual standard deviations are given in Supplementary 2. In the present work, 77 out of all the reviewed 111 articles reported experimental errors, which refer to 4328 data points including 477 data sets. When experimental errors were not reported in the original article, we assigned the following systematic experimental errors to the data: 1 cm/s absolute standard deviation for the CTF, HFM, and SJF methods, 5% relative standard deviation for the OPF and HDC methods, and 6% relative standard deviation for the FCM method. The details of the determination of these uncertainties are discussed in Part 4 of Supplementary 1.

If low experimental error $\sigma_{\mathrm{exp},ij}$ was estimated by the original authors and the statistical error $\sigma_{\mathrm{stat},i}$ is also very low for a data series due to the low scatter of data points around their trendline, then the estimated composite standard deviation σ_{ij} is also very low, which would lead to amplified, unrealistically high error function values E. Therefore, a minimum limitation of the standard deviation of measurements is needed. We selected the minimum composite standard deviation as 1% of the experimental LBV, but at least 0.5 cm/s. This minimum standard deviation was enforced for 776 data points of the total 5500 data points.

Combining the regions of applicability with the uncertainty of the measurements, more details are obtained. Figure 2 shows that methods SJF and HFM have the lowest absolute uncertainty, in accordance with that these techniques were used for measuring relatively small LBVs. FCM and HDC have the highest average absolute uncertainties, and OPF also has large average uncertainty, and

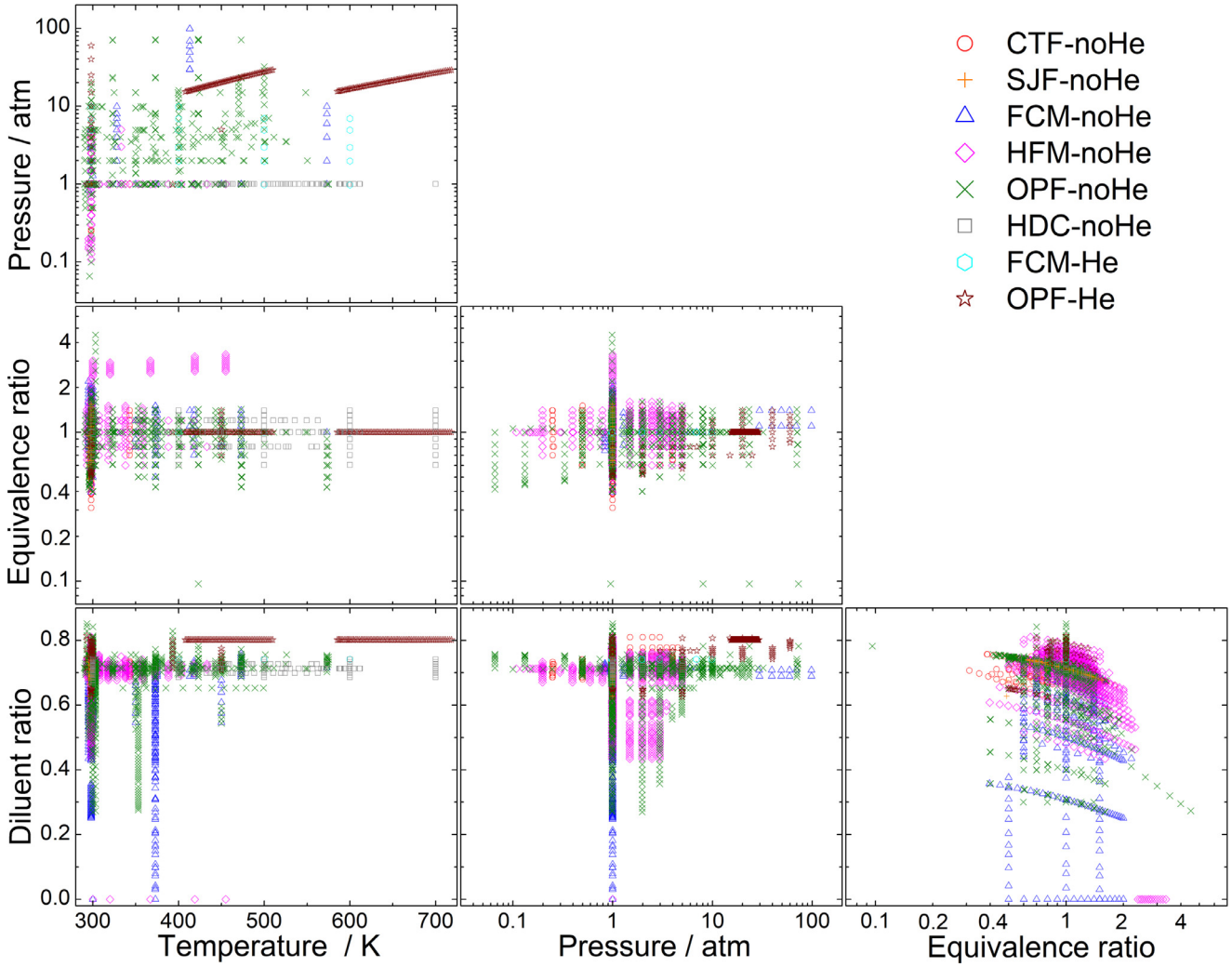

Fig. 1. Distribution of the cold side temperature, pressure, equivalence ratio and diluent ratio in the collected LBV measurements. The legends indicate the various methods and the application of helium diluent (-He/-noHe).

these were used to measure large LBVs. As for the CTF method, it has the highest relative uncertainty, but has a quite narrow range for measured LBVs.

4. The investigated mechanisms

In the present study, we investigated 12 widely used methane combustion mechanisms. The mechanism identifiers were created by combining the names of the mechanism or the group-leading authors and the years of publication. These are GRI3.0-1999 [5], USC-II-2007 [4], Konnov-2009 [6], SanDiego-2014 [37], CRECK-2014 [38], Caltech-2015 [39], Aramco-II-2016 [10], SanDiego-2016 [3], FFCM-I-2016 [11], Konnov-2017 [40], Glarborg-2018 [41], NUIG1.1-2021 [42], respectively. Except for NUIG1.1-2021, the other 11 mechanisms are among the 13 mechanisms that had been studied in our recent article [1]. Two mechanisms were not studied here: the GDF-2012 was omitted, because no transport data were provided with this mechanism and furthermore this mechanism was developed to describe ignition delay time measurements [43]. Results of the Leeds-2001 mechanism are not reported here, as convergence issues occurred during the simulations. The diagnostics tool of Cantera identified that the reasons of the numerical problems were the too high values of some rate coefficients at low temperatures. The k values of the following reactions are significantly high at 300 K: $CH_2CO + M = H + HCCO + M$ (k_{rev} = 7.52e+80), $C_2H_2 + CH = C_2H + CH_2$ (k_{rev} = 1.79e+36), $C_2H_2 + M = C_2H + H + M$ (k_{rev} = 1.08e+30), $CH_3 + M = CH_2 + H + M$ (k_{rev} = 2.08e+25), $CH_2CO + M = CH_2 + CO + M$ (k_{rev} = 7.21e+23). The units of the rate coefficients are $cm^3\ mole^{-1}\ s^{-1}$.

All the investigated mechanisms were validated on methane combustion data by their authors and also all mechanisms, but the two SanDiego mechanisms, were validated on methane laminar burning velocity measurements by their developers. In the Supplementary, Table B lists the range of conditions (temperature, pressure, equivalence ratio (φ) and diluent ratio) of their validating LBV measurements, whereas Fig. 3 plots these ranges. The cold side temperatures of the validating measurements for USC-II-2007, Konnov-2009, Caltech-2015, Konnov-2017, NUIG1.1-2021 were around room temperature (290–300 K), whereas for the other mechanisms higher temperatures were also used (300–480 K). Regarding pressures, the validating simulations for USC-II-2007 were done only at atmospheric condition, while the other mechanisms were validated also at higher pressures (1 – 20 atm), except for Konnov-2009, which was tested at both low and high pressures (0.25–10 atm). The ranges of equivalence and diluent ratios in the validating measurements for the 12 mechanisms are very similar, they are in the ranges of 0.5 – 1.6 and 65–81%, respectively. In both panels of Fig. 3, the last pairs of columns represent the condition ranges of the experimental data collected in

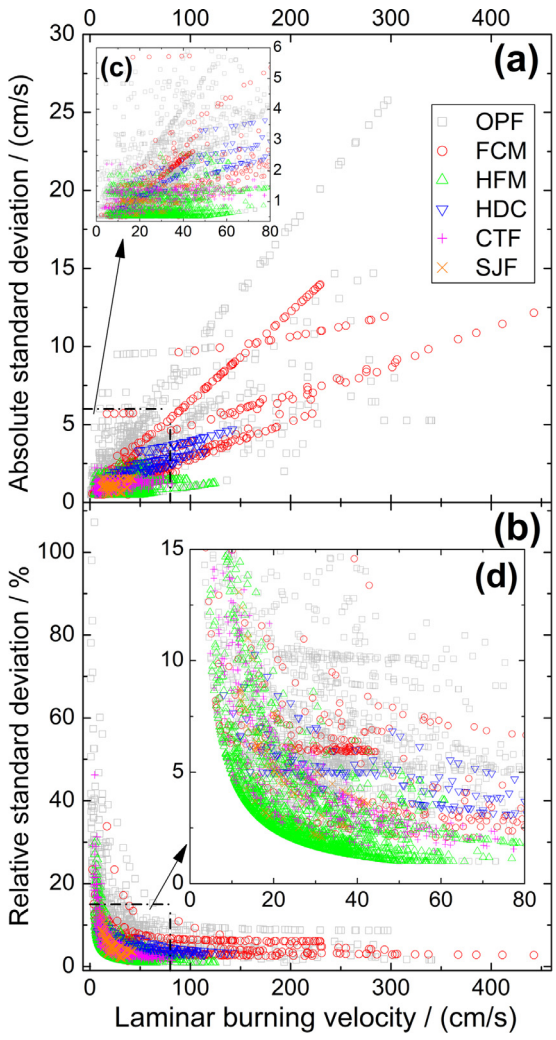

Fig. 2. Relation between the uncertainty of the measurements and the magnitude to the LBV for all the measurements without helium. Panel (a) shows the estimated absolute standard deviation (cm/s, left axis) vs. laminar burning velocity and panel (b) shows the relative (%, right axis) standard deviation (absolute standard deviation / LBV) vs. laminar burning velocity. Panels (c) and (d) enlarge the densest regions within the same panel.

the present study. We also found a data set with equivalence ratio of 0.096, however, it was not used for the tests as none of the mechanisms could reproduce it to an acceptable degree. Therefore, as shown in Fig. 3b, the lowest equivalence ratio of the measurements used for the mechanism evaluation is 0.31. The ranges of testing conditions are much wider than those of the validating simulations for any of the mechanisms, therefore this study provides new information for all mechanisms.

5. Details of simulations

All LBV experimental data were encoded in ReSpecTh Kinetics Data Format v2.3 (RKDF2.3) [19] XML files. The RKD format is an XML data format for the storage of indirect combustion measurements and rate coefficient determinations by direct gas kinetics measurements and theoretical calculations. The RKD format is a modified and extended version of the PrIMe Kinetics Data Format [44]. All the prepared XML files are available in the ReSpecTh database (http://respecth.hu/) [18].

The RKD files contain all information required for the simulation of the experiments, such as initial compositions, temperature and pressure. In principle, the complete testing of a mechanism against several thousand experimental data points can be carried out in a single run based on these files using the Optima++ framework [45]. In the present study, the OpenSMOKE++ [46,47] (OS) simulation package was used in the Optima++ environment for simulating LBVs. To check the results, many experiments were also simulated with FlameMaster [48]. There were only minor differences between the LBVs calculated by these two simulation packages. The average absolute difference between the LBVs calculated by the two codes was 0.67 cm/s, based on 1271 simulations. The simulated LBV value for the j-th data point of the i-th data set (y_{ij}^{sim}) is denoted with $v_{\mathrm{L},ij}$.

Some experimental data points could not be reproduced within 3σ error by any of the investigated mechanisms. We assume that most of these data have large systematic errors, but it is possible that some of them are related to special conditions that none of the current mechanisms can handle. To avoid biased conclusions, we excluded these data sets from testing. In addition, using measurements without correction for stretch or heat-loss may result in incorrect conclusions, therefore we excluded the data with missing stretch or heat-loss correction. In these ways, 152 data sets containing 1086 data points in total, were identified, and excluded from the comparison. These excluded datasets were indi-

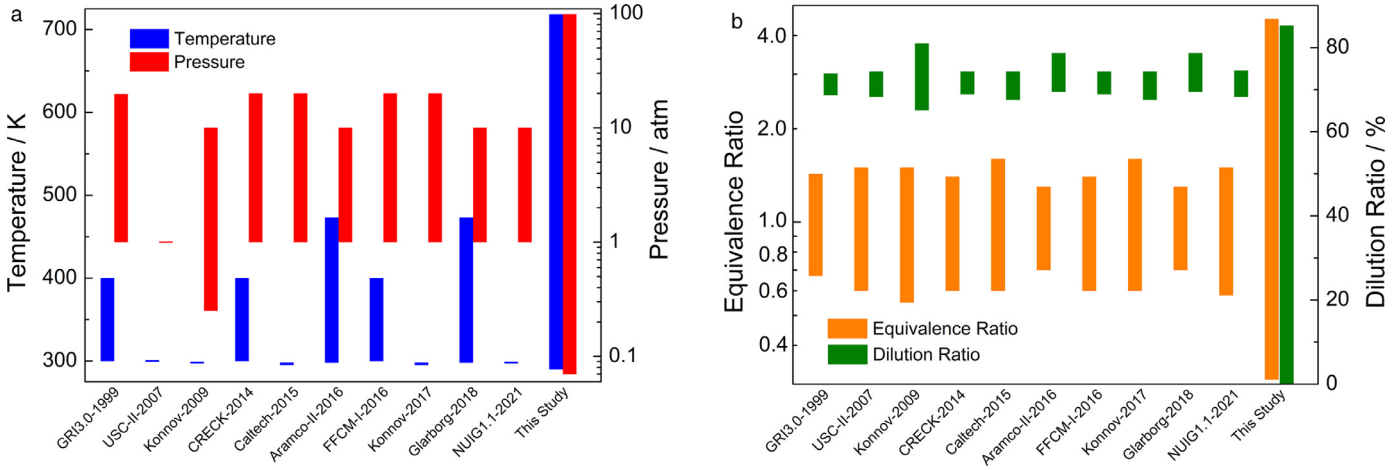

Fig. 3. Comparison of temperature, pressure, equivalence ratio and diluent ratio ranges of methane LBV measurements originally used for the validation of 10 of the 12 mechanisms with those of the experimental data used in this study. Mechanisms SanDiego-2014 and SanDiego-2016 are not included as they were not validated against methane LBV data by their developers.

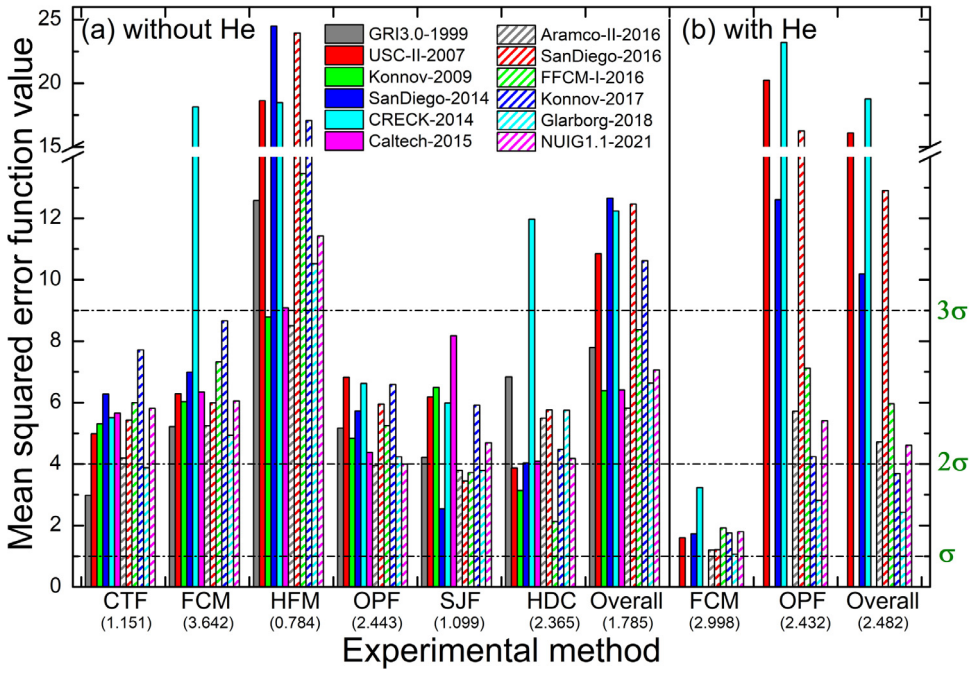

Fig. 4. Mean squared errors of the mechanisms in reproducing LBVs for measurements (a) without helium and (b) with helium diluent, for each experiment type and for all measurements. The experiment types are: CTF: counterflow twin-flame method, FCM: flame cone method, HFM: heat flux method, OPF: outwardly propagating flame method, SJF: single jet flame, HDC: externally heated diverging channel method. The numbers given in parentheses below the measurement types are the average of the estimated error (σ) of the corresponding experimental LBV values, in cm/s units.

cated by either grey or yellow shading in Table A of the Supplementary. Testing of the mechanisms was based on the remaining 4414 data points in 494 data sets (4174 data points / 476 datasets are for helium-free measurements, 240 data points / 18 datasets for helium-including measurements).

For three mechanisms with the lowest E error values, local sensitivity analysis [49] was carried out at the conditions of each LBV measurement. Sensitivity coefficients, $S_{ij,k} = d\nu_{\mathrm{L},ij}/\mathrm{d}A_k$, were calculated using the finite difference formula via repeated simulations with +5% perturbation in Arrhenius parameter A_k of reaction step k. Normalized sensitivities were calculated using equation $\mathrm{d}\ln\nu_{\mathrm{L},ij}/\mathrm{d}\ln A_k = (A_j/\nu_{\mathrm{L},ij})\ \mathrm{d}\nu_{\mathrm{L},ij}/\mathrm{d}A_k$. The normalized sensitivity coefficients were scaled to values between −1 and +1 by dividing them with the absolute value of the largest absolute sensitivity coefficient for each data point. The most influential reactions for the reproduction of each data point were identified based on the order of the absolute values of the scaled normalized sensitivity coefficients. Furthermore, range [−1, +1] was divided into ten equidistant intervals, and the relative frequency of the reactions in each interval considering all data points was counted and investigated.

6. Results and discussion

6.1. Performance comparison of the mechanisms by measurement types

Figure 4 shows the mean squared error function value (E) of the mechanisms separately for mixtures with (a) and without (b) helium bath gas considering all measurements, and also according to the various measurement types.

At the calculations of the E and D values, the deviation between the simulated and experimental data is divided with the estimated uncertainty of the data point, which means that usually a higher deviation is tolerated for an FCM data point compared to an SJF data point. The consequence is that there are usually no big differences among the E values for the same mechanism for the data obtained from the six experimental techniques. Also, Konnov et al. [2] commented that the recent experimental data reported with different methods and various stretch extrapolations techniques match well with non-stretched flames for CH_4/O_2/diluent mixtures. This also means that it is justified to investigate the performance of the mechanisms at various conditions based on all data points, without separating the measured LBV values according to the experimental method.

It is interesting that the earliest mechanism, the two-decade old GRI3.0-1999 can reproduce all kinds of LBV data relatively well, within 3σ error (E<9). According to Fig. 4 and Table 2, mechanisms Aramco-II-2016 and Konnov-2009 can reproduce the LBV data without helium diluent from all types of measurements with about 2.4σ experimental error on average. Glarborg-2018 and Caltech-2015 also show a similar level of accuracy, except for the data from HFM measurements. Considering the measurements without helium diluent, all mechanisms reproduce the CTF, OPF and SJF data well with a mean standard error of about 2σ ($E = 4$) and always with less than 3σ (E<9). Except for the CRECK mechanism, all mechanisms reproduce the FCM and HDC data with similarly good accuracy and with a mean standard error less than 3σ. Considering the experiments using helium diluent, Glarborg-2018 and Konnov-2017 can reproduce the LBV data within 2σ experimental error (E<4), and the E values of NUIG1.1-2021, Aramco-II-2016 and FFCM-I-2016 are within 3σ (E<9). However, GRI3.0-1999, Konnov-2009 and Caltech-2015 do not contain helium as an option for bath gas.

Figure 5 shows the mean signed deviation D with $\pm 2\sigma_D$ error bars, for all mechanisms according to the experiment types and for all LBV measurements with and without helium diluent. Except for the smallest D values, the σ_D values are significantly smaller than the D values, thus we may speak about systematic under- or over-prediction for most of the cases with high statistical confidence. For the CTF, FCM, HFM and OPF measurements without helium, all mechanisms but CRECK-2014 and GRI3.0-1999 underpre-

Table 2
The mean squared error function values E for all the mechanisms. The shaded cells indicate the errors of the three best performing mechanisms in each experimental type. Three derived mechanisms (K + R28 (Konnov-2009+R28); C + R28 (Caltech-2015+R28); F + R29 (FFCM-I-2016+R29), see Section 6.5) are also included; in these rows bold numbers indicate when the modified mechanism is better than the original one.

No.	Mechanisms ID	without He							with He		
		CTF	FCM	HFM	OPF	SJF	HDC	Overall	FCM	OPF	Overall
1	GRI3.0-1999	2.980	5.219	12.582	5.170	4.217	6.832	7.790	-	-	-
2	USC-II-2007	4.988	6.284	18.633	6.826	6.184	3.872	10.846	1.599	20.238	16.096
3	Konnov-2009	5.310	6.029	8.785	4.837	6.490	3.139	6.385	-	-	-
4	SanDiego-2014	6.277	6.991	24.494	5.729	2.539	4.039	12.655	1.729	12.606	10.189
5	CRECK-2014	5.509	18.145	18.477	6.624	5.987	11.973	12.239	3.232	23.201	18.763
6	Caltech-2015	5.658	6.345	9.085	4.378	8.177	4.085	6.412	-	-	-
7	Aramco-II-2016	4.192	5.242	8.500	3.949	3.788	5.496	5.816	1.201	5.719	4.715
8	SanDiego-2016	5.431	5.993	23.941	5.954	3.449	5.759	12.464	1.215	16.242	12.903
9	FFCM-I-2016	5.998	7.323	13.453	5.245	3.719	2.125	8.372	1.919	7.118	5.963
10	Konnov-2017	7.715	8.666	17.073	6.585	5.916	4.475	10.618	1.755	4.238	3.686
11	Glarborg-2018	3.876	4.935	10.521	4.234	3.785	5.751	6.631	1.064	2.82	2.430
12	NUIG1.1-2021	5.814	6.057	11.424	3.998	4.694	4.181	7.057	1.800	5.409	4.607
13	K+R28	**4.515**	**4.816**	**7.799**	5.322	**4.843**	4.800	**6.098**	-	-	-
14	C+R28	**4.175**	**5.043**	**7.168**	4.486	**5.581**	5.679	**5.558**	-	-	-
15	F+R29	**3.430**	**4.169**	**7.266**	**4.749**	6.066	5.201	**5.553**	2.021	10.244	8.417

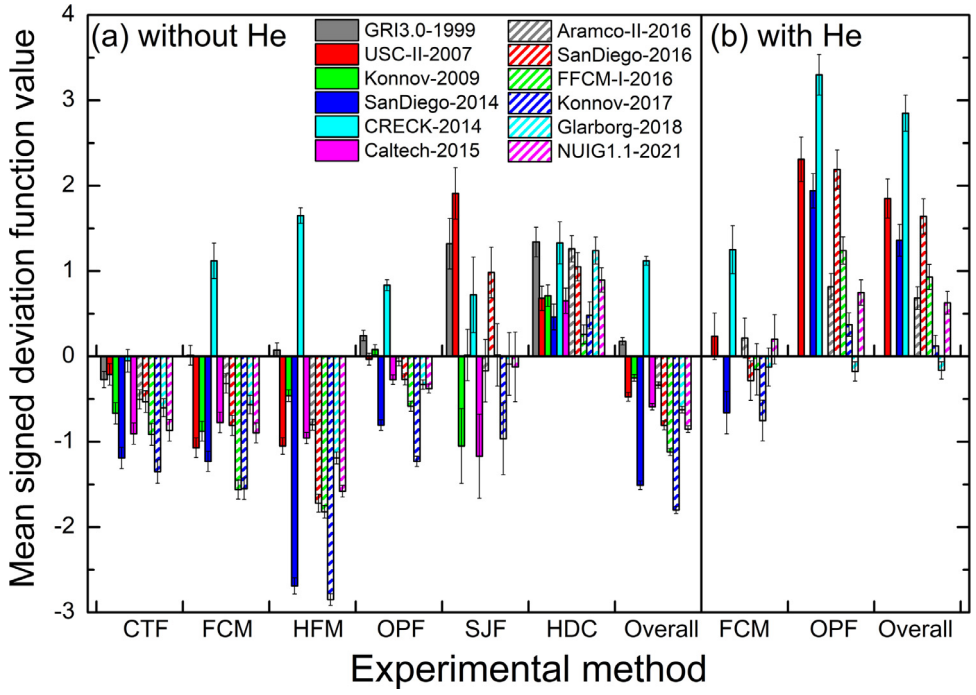

Fig. 5. Mean signed deviation value D with $\pm 2\sigma_D$ error bars, for all mechanisms according to the experiment types and for LBV measurements with and without helium.

dict the measured values. For the HDC measurements, all mechanisms on average overpredict the LBV values. There is no systematic deviation concerning the mechanisms for the SJF measurements. Regarding the measurements with helium bath gas, most mechanisms overpredict the OPF measurements, and there is no systematic tendency for the FCM measurements.

Figure 6, panels a and b, display the average Pearson correlation coefficients between the mechanisms considering all data points, without and with helium bath gas, respectively. Like in the previous similar investigations [21,22], the correlations among the signed simulation errors of data points show which mechanisms are intrinsically similar. For the LBV experimental data without he-

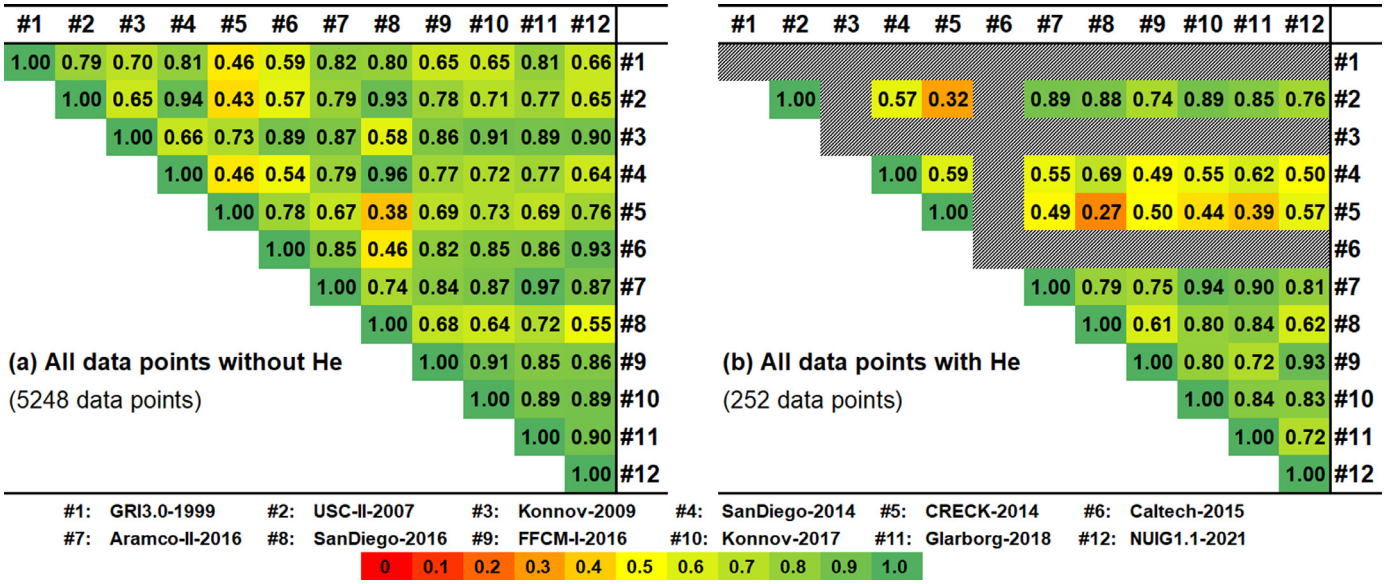

Fig. 6. Matrix of Pearson correlation coefficients between the signed simulation errors of the mechanisms regarding all LBV experimental data. All correlation coefficients are positive. Mechanisms GRI3.0-1999, Konnov-2009 and Caltech-2015 do not contain helium, therefore the corresponding columns and rows are empty in the right panel.

lium, SanDiego-2014 (#4) and SanDiego-2016 (#8) always provide similar results, and these are also similar with those of USC-II-2007 (#2). There is also a strong correlation between mechanisms Aramco-II-2016 (#7) and Glarborg-2018 (#11), and the results from this pair of mechanisms are fairly well correlated with those of mechanisms GRI3.0-1999 (#1), Konnov-2009 (#3), Caltech-2015 (#6), FFCM-I-2016 (#9), Konnov-2017 (#10), NUIG1.1-2021 (#12). This essentially means that the 12 mechanisms can be separated into two groups and it is only CRECK-2014 (#5) that does not provide results similar to the others. Considering the experiments with helium (Fig. 6b), the correlations are much weaker, but there are still fair correlations in the two mechanism sets, USC-II-2007 (#2) / Aramco-II-2016 (#7) / SanDiego-2016 (#8) / Konnov-2017 (#10) / Glarborg-2018 (#11) and FFCM-I-2016 (#9) / NUIG1.1-2021 (#12).

6.2. Comparison of mechanism performance under various conditions

Figure 7a shows the mean squared error values belonging to the various cold side temperature intervals from room temperature to 612 K. For all mechanisms, the E values do not change much with increasing temperature up to 500 K. Above 500 K cold side temperature, the error function values start to increase for all mechanisms, although these E values just slightly exceed 3σ for mechanisms NUIG1.1-2021, Aramco-II-2016, and Caltech-2015. Figure 7b presents error function value E as a function of pressure on a logarithmic scale. Most mechanisms have high error at low pressures ($p < 0.5$ atm), very good performance for pressures between 0.5 and 1.0 atm and acceptable error near atmospheric pressure. The performance of several mechanisms is improving with increasing pressure, starting from atmospheric pressure.

Figure 7c shows the errors of mechanisms for various equivalence ratio (φ) intervals. The mean squared errors show the same pattern for most mechanisms, that is the accuracy of the prediction of LBV is very good for fuel-lean and stoichiometric mixtures, but for fuel-rich mixtures the errors are high. In the range of $\varphi = 0.85-0.99$, almost all mechanisms reproduce the experimental data within 3σ on average. The probable reason is that at fuel-lean and stoichiometric conditions the laminar burning velocity is controlled by the C1 chemistry. The rate parameters of the corresponding reaction steps are known with low uncertainty. The laminar burning velocities of fuel-rich flames are partially controlled by the C2 oxidation chain of methane oxidation, and the corresponding rate parameters are known with higher uncertainty. Figure 7c shows that all mechanisms have a poor prediction (above 3σ, E<9) in the equivalence ratio range $1.25 < \varphi < 1.55$. Mechanism Konnov-2009 is much better in this range than the other ones. Interestingly, the E error function values of almost all mechanisms start to improve above $\varphi = 1.55$ and become really low above $\varphi = 2$. Increasing the diluent ratio (Fig. 7d), the general tendency is that the error of all mechanisms decrease.

Figure S2 of the Supplementary shows the average mean signed deviation values of the mechanisms in various intervals of cold side temperature, pressure, equivalence ratio, and diluent ratio based on LBV measurements without helium bath gas. The variations of systematic errors as a function of the four condition parameters show that most mechanisms systematically underpredict, or overpredict the calculated laminar burning velocity. Usually there is no such single sided bias for mechanisms Aramco-II-2016, Konnov-2009, FFCM-I-2016, SanDiego-2016, and USC-II-2007.

In Figs. 7 and S2, each interval of experimental conditions contained typically several hundred, the most frequent ones (e.g. near $T = 300$ K and $p = 1$ atm) even several thousand data points. This means that the conclusions are not sensitive to the individual errors of the data points for the LBV experimental data that used diluent without helium.

Figures S3 and S4 present the variations of the E and D values, respectively, in a similar way in the various intervals of experimental conditions based on LBV measurements with helium diluent gas. As the numbers at the top of the columns in Fig. S3 show, in this case each interval contains only a few, at most a few dozens of measurements. Therefore, it is better not to draw detailed conclusions from these figures. In general, Glarborg-2018, Aramco-II-2016, NUIG1.1-2021, and Konnov-2017 reproduce the experimental data with helium bath gas the best, and also they do not show one-sided bias in the whole intervals.

6.3. Conditions of a natural gas engine

Natural gas engines are widely used in trucks and town buses. In these engines typically near stoichiometric mixtures are applied and the pollutants are removed from the exhaust gas by three-way

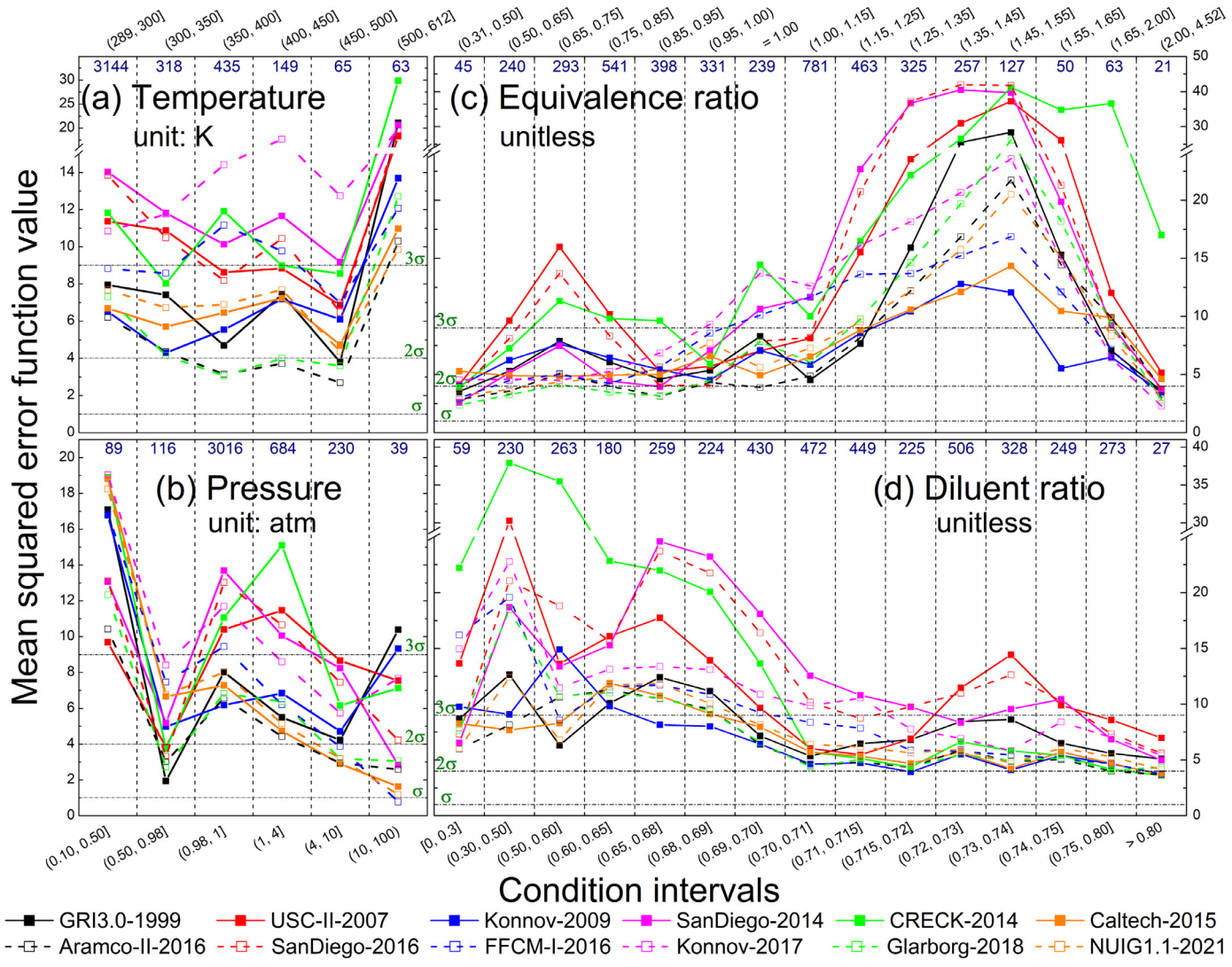

Fig. 7. Average error function values of the mechanisms in various intervals of (a) temperature, (b) pressure, (c) equivalence ratio, (d) diluent ratio based on LBV measurements without helium bath gas. The numbers on the top of the intervals indicate the numbers of data points used.

catalysts. Natural gas engines are also used for electricity production and marine transportation [50]. Some of these engines also apply stoichiometric mixtures, while most of such engines use a lean mixture (air–fuel equivalence ratio $\lambda = 1.1 - 1.7$; fuel–air equivalence ratio $\varphi = 0.91-0.58$). Furthermore, utilization of pre-ignition chambers allows the application of ultra-lean mixtures ($\lambda = 2.1 - 2.2$; $\varphi = 0.48-0.45$) [51]. When lean or ultra-lean mixtures are used, the exhaust gas contains very little CO and NOx, therefore the application of three-way catalysts is not needed.

In spark ignition engines the fresh mixture is compressed by the piston and after the ignition the flame front is spreading in a high-temperature – high-pressure mixture. D'Adamo [52] demonstrated that in gasoline engines the flame is spreading in a fresh mixture that can be characterized by a narrow band of correlated temperature and pressure, even when the size of the engine architecture and engine speed were changed in a very wide range (see Fig. 1 in [52]). Following this idea, Wang et al. [17] derived a similar, highly correlated band of possible pressure and temperature values of a compressed stochiometric methane–air mixture for natural gas engines. The band is determined by the isentropic compression relationship, $T_u/T_{u,0} = (p/p_0)^{1-1/\gamma}$, where $T_{u,0}$ and p_0 are the initial temperature and pressure, respectively, and γ is the specific heat capacity ratio of unburned gas. Considering that in the natural gas engines the mixtures are not always stochiometric, we plotted the isentropic bands for CH_4–air mixtures with both lean ($\varphi = 0.5$) and stochiometric ($\varphi = 1.0$) equivalence ratios. As shown in Fig. S5, the locations of the bands are negligibly shifted with changing equivalence ratios. Wang et al. [17] did not find any literature methane LBV measurements in this (p, T) region and therefore carried out own measurements with a stoichiometric mixture using the OPF method. To suppress flame instability at high pressures, N_2/He mixture was used as diluent in higher ratio compared to air. Wang et al. [17] investigated the performance of 7 mechanisms and found that FFCM-1 (FFCM-I-2016) provided simulation results most closely to their own experimental data.

Since our methane LBV experimental data collection is very comprehensive, we expected that it contained measurements also at the conditions of natural gas engines. Unfortunately, we also did not find data in this region and therefore we used the data of Wang et al. for a similar testing.

As shown in Fig. 8, FFCM-I-2016, NUIG1.1-2021, and SanDiego-2014 very well reproduced the experimental data of Wang et al. [17]. The simulated LBVs obtained with SanDiego-2016, Aramco-II-2016 and Konnov-2017 are also within the 2σ error limits. Note, that Fig. 6b of article [17] showed 1σ error bars and these were reproduced in Fig. 8 as 2σ error bars.

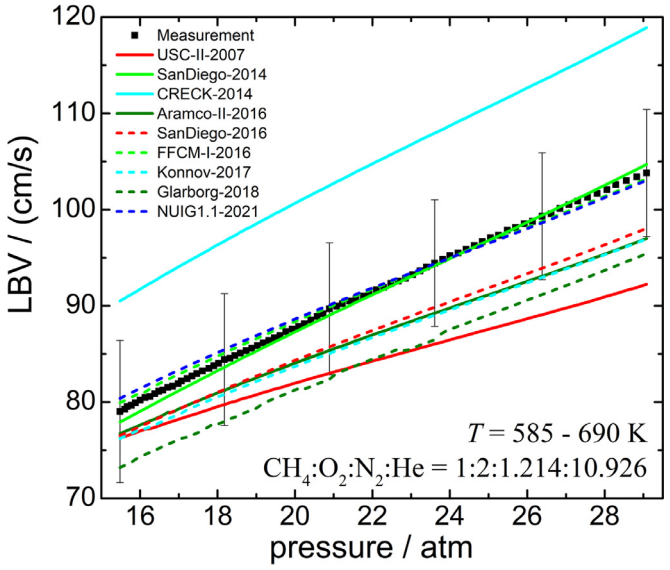

Fig. 8. Measured and simulated laminar burning velocities of a stoichiometric methane-containing mixture under the conditions relevant for natural gas engines. The experimental data and their estimated 2σ errors were published by Wang et al. [17]. Simulated LBVs are given for all mechanisms, but GRI3.0-1999, Konnov-2009 and Caltech-2015, which do not contain He as a diluent.

6.4. Sensitivity analysis

Aramco-II-2016 and Konnov-2009 have the lowest E values for measurements without helium, and Glarborg-2018 has low error function values for measurements both with and without helium. Therefore, we carried out sensitivity analyses based on these three mechanisms for methane/air mixtures under 18 typical cold side conditions (T: 300 / 400 K, p: 0.2 / 1 / 60 atm, φ: 0.5 / 1.0 / 2.0). We selected the top 20 reactions with the highest absolute scaled sensitivity coefficients for each mechanism, and due to the overlap, it provided a list of 29 important reactions (see Table 3). The absolute scaled sensitivity coefficients of the reactions are available in Table C of the Supplementary.

The following analysis is based on these 29 important reactions. In Figs. 9-11, for the 29 important reactions, we compared the Arrhenius curves of the rate coefficients used in all the 12 mechanisms with the available direct experimental and theoretical data over the temperature range of 550–2850 K. Further information about the rate parameters used in the models, the related direct measurements and theoretical results are available in the *k-evaluation* web site [53].

Several of these reactions belong to the hydrogen oxidation system (R1 H + O_2 = OH + O; R3 H + O_2 (+ M) = HO_2 (+ M) (LP, M = N_2); R4 HO_2 + OH = H_2O + O_2; R11 H_2 + OH = H_2O + H, R25 H_2 + O_2 = HO_2 + H) or the carbon-containing reactions of the syngas oxidation system (R2 CO + OH = CO_2 + H; R5 HCO (+ M) = H + CO (+ M) (LP, M = N_2); R8 HCO + O_2 = CO + HO_2). We have discussed the selection of the rate parameters of these reactions in our earlier publications [54,55,56] and therefore these will not be detailed here. Some other reaction steps belong to the methanol/formaldehyde oxidation system: R6 CH_3 + HO_2 = CH_3O + OH; R12 CH_2O + HO_2 = HCO + H_2O_2; R17 CH_2O + OH = HCO + H_2O; R26 CH_2O + H = HCO + H_2; R27 CH_3OH (+ M) = CH_3 + OH (+ M) (LP, M = N_2); R29 CH_2O + H = CO + H_2 + H), which has also been discussed in details in one of our previous works [23]. The discussion of reactions R7 CH_4 + OH = CH_3 + H_2O, R9 CH_3 + O_2 = CH_2O + OH and R18 CH_4 + HO_2 = CH_3 + H_2O_2 has been carried out in the methane – ignition delay time study [1]. The rate parameters of these reactions also will not be conferred here in details either.

Table 3
Important reactions (denoted by √) identified by sensitivity analysis of the Konnov-2009 (K), Aramco-II-2016 (A) and Glarborg-2018 (G) mechanisms. Reactions missing from any of these three mechanisms are indicated by 0.

	Reactions	K	A	G
R1	H + O_2 = OH + O	√	√	√
R2	CO + OH = CO_2 + H	√	√	√
R3	H + O_2 (+ M) = HO_2 (+ M) (LP, M = N_2)	√	√	√
R4	HO_2 + OH = H_2O + O_2	√	√	√
R5	HCO (+ M) = H + CO (+ M) (LP, M = N_2)	√	√	√
R6	CH_3 + HO_2 = CH_3O + OH	√	√	√
R7	CH_4 + OH = CH_3 + H_2O	√	√	√
R8	HCO + O_2 = CO + HO_2	√	√	√
R9	CH_3 + O_2 = CH_2O + OH	√	√	√
R10	CH_4 (+ M) = CH_3 + H (+ M) (LP, M = N_2)	√	√	√
R11	H_2 + OH = H_2O + H	√	√	√
R12	CH_2O + HO_2 = HCO + H_2O_2	√	√	√
R13	C_2H_6 (+ M) = CH_3 + CH_3 (+ M) (HP)	√	√	
R14	CH_3 + O = H + CH_2O	√		√
R15	CH_2 + O_2 = CO_2 + H + H	√		√
R16	CH_3 + HO_2 = CH_4 + O_2		√	√
R17	CH_2O + OH = HCO + H_2O		√	√
R18	CH_4 + HO_2 = CH_3 + H_2O_2		√	√
R19	CH_3 + H (+ M) = CH_4 (+ M) (HP)		√	√
R20	CH_2(S) + H_2O = CH_3OH	√		
R21	CH_3 + O_2 = CH_3O + O	√		
R22	CH_2(S) + O_2 = CO + OH + H	√		0
R23	CH_3 + OH = CH_2(S) + H_2O	√		
R24	CH_4 + H = CH_3 + H_2	√		
R25	H_2 + O_2 = HO_2 + H		√	
R26	CH_2O + H = HCO + H_2		√	
R27	CH_3OH (+ M) = CH_3 + OH (+ M) (LP, M = N_2)		√	*
R28	CH_3 + O = H_2 + CO + H	0	0	√
R29	CH_2O + H = CO + H_2 + H	0	0	√

LP: low-pressure limit, HP: high-pressure limit. S: singlet.
*low-pressure rate coefficients were defined with the PLOG formalism.

In the following paragraphs, we will mainly concentrate on the reaction steps specific to methane flames (not sharing importance with the hydrogen, syngas, methanol and formaldehyde combustion systems) and especially on the usage of the rate parameters in reaction mechanisms Konnov-2009, Caltech-2015, Aramco-II-2016, NUIG1.1-2021 and Glarborg-2018.

In Fig. 9, the rate coefficients of reactions H + O_2 = OH + O (R1), HCO (+ M) = H + CO (+ M) (LP, M = N_2) (R5), CH_4 + OH = CH_3 + H_2O (R7) and H_2 + OH = H_2O + H (R11) in all mechanisms match the directly measured experimental rate coefficients accurately.

For reaction CH_3 + HO_2 = CH_3O + OH (R6), Glarborg-2018 takes Arrhenius parameters from the theoretical study of Jasper et al. [57], around which the measured rate coefficients are distributed. Most mechanisms use rate parametrizations that are consistent with the experimental data.

While the Arrhenius curve of HCO + O_2 = CO + HO_2 (R8) in most mechanisms runs within the wide uncertainty range of experimental data, only those of Konnov-2017 and Glarborg-2018 capture well the trend of measurements. This seems to indicate that the rate parameters of reactions R6 and R8 as used in Glarborg-2018 are more reliable.

In all mechanisms except USC-II-2007, the rate parametrizations of reaction CH_3 + O_2 = CH_2O + OH (R9) agree well with the experimental data that are only available at high temperatures (>1250 K). Whereas at lower temperatures, where we have no experimental data, the rate coefficients of R9 are rather different in the various mechanisms.

The available directly measured rate coefficients for CH_4 + M = CH_3 + H + M (LP, M = N_2) (R10) are concentrated at the high temperatures (>1650 K), the rate parameterization in all mechanisms agreed very well with them, and also with each other in the whole temperature range.

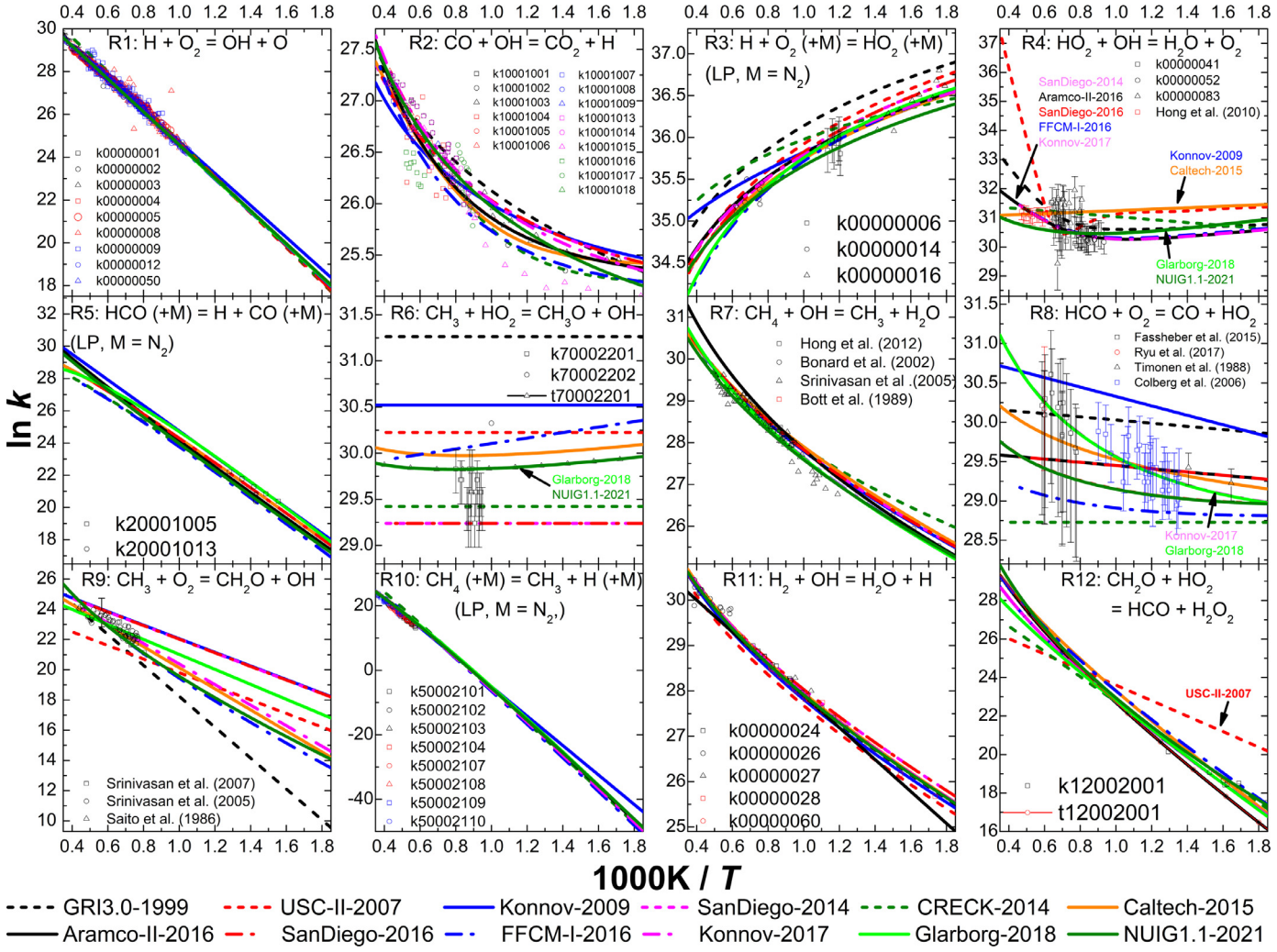

Fig. 9. Comparison of the rate parametrizations of important reactions R1 - R12 with the available direct determinations. The units of the rate coefficients are expressed in cm, mol and s units. The ID numbers for the direct measurements are identical to those in the ReSpecTh database and the detailed references are available in the Supplementary. More direct measurement data are used: Hong et al. (2010) [58] for R4, Hong et al. (2012) [59], Bonard et al. (2002) [60], Srinivasan et al. (2005) [61] and Bott et al. (1989) [62] for R7, Fassheber et al. (2015) [63], Ryu et al. (2017) [64], Timonen et al. (1988) [65] and Colberg et al. (2006) [66] for R8, Srinivasan et al. (2007) [67], Srinivasan et al. (2005) [68] and Saito et al. (1986) [69] for R9. Scatter points: experimental direct determination of the rate coefficients, thin solid line with points: theoretical direct determination of the rate coefficients.

For all mechanisms but USC-II-2007 and CREC-2014, the Arrhenius curves of $CH_2O + HO_2 = HCO + H_2O_2$ (R12) run close to each other and they are well in line with the direct measurements. This is not true for USC-II-2007 in the whole temperature range and for CREC-2014 at high temperatures (T>1200 K). This indicates that the rate parameters used in these mechanisms are well established.

In Fig. 10, the Arrhenius curves both for reaction C_2H_6 (+ M) = CH_3 + CH_3 (+ M) (HP) (R13) and for reaction $CH_4 + HO_2 = CH_3 + H_2O_2$ (R18) are running close to each other for all mechanisms and also close to the experimental data (available only for R13).

For $CH_3 + O = H + CH_2O$ (R14), only a few points of direct measurements are available in the investigated temperature range, with which the Arrhenius curves for the majority of the mechanisms are consistent, except for Caltech-2015, GRI3.0-1999 and FFCM-I-2016 that employ slightly lower rate coefficients. Parametrizations in all mechanisms agree well with each other as they have only very little or no temperature dependence and they span a narrow range.

No direct experimental data are available for reaction $CH_2 + O_2 = CO_2 + H + H$ (R15). The Glarborg-2018 mechanism, which identified R15 as sensitive, adopted its Arrhenius parameters from unpublished work of Klippenstein et al. However, in Fig. 10 it is seen that GRI3.0-1999, Konnov-2009, NUIG1.1-2021, Aramco-II-2016 and FFCM-I-2016 have used similar rate coefficients for R15.

For mechanisms USC-II-2007, CRECK-2014, Konnov-2009, SanDiego-2014 and SanDiego-2016, the Arrhenius curves of $CH_3 + HO_2 = CH_4 + O_2$ (R16), are running below the measured rate coefficient values. The rate parametrization in Caltech-2015, Aramco-II-2016, FFCM-I-2016 and Konnov-2017 adapted the theoretical results of Jasper et al. [57] which is consistent with the experimental values. The rate coefficient curves in Glarborg-2018 and NUIG1.1-2021 are slightly above the theoretical curve, nevertheless, it is also consistent with the measured values.

Direct measurements for R17 ($CH_2O + OH = HCO + H_2O$) have obvious discrepancy, resulting in a wide uncertainty band which covers relatively well the scattered Arrhenius curves of the dif-

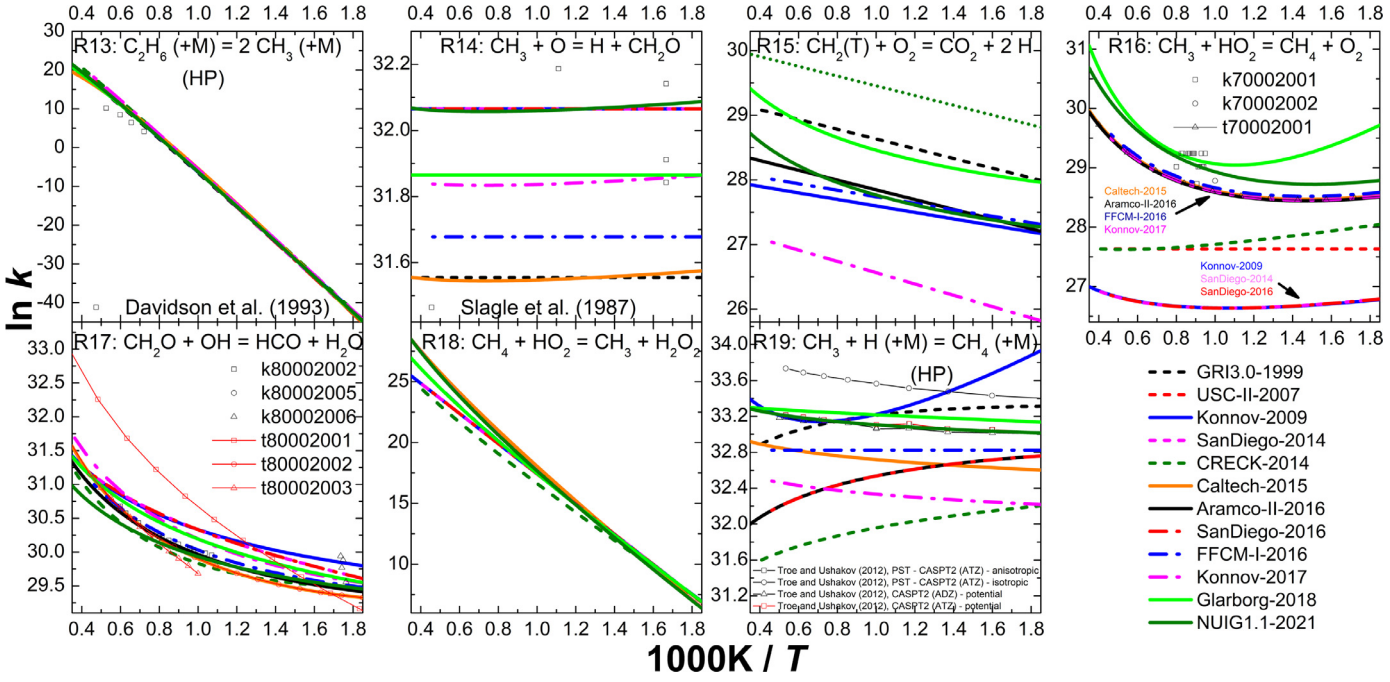

Fig. 10. Comparison of the rate parametrizations of important reactions R13 - R19 with the available direct determinations. The units of the rate coefficients are expressed in cm, mol, s. The ID numbers for the direct measurements are identical to the ReSpecTh database, the detailed reference is available in the Supplementary. More direct measurement data are used: Davidson et al. (1993) [70] for R13, Slagle et al. (1987) [71] for R14, Tore and Ushakov (2012) [72] for R19. Scatter points: experimental direct determination of the rate coefficients, thin solid line with points: theoretical direct determination of the rate coefficients.

ferent mechanisms in the investigated temperature range. Mechanisms GRI3.0-1999 and USC-II-2007 do not contain R18.

Tore and Ushakov [72] provided theoretical results for reaction $CH_3 + H (+ M) = CH_4 (+ M)$ (HP) (R19). Glarborg-2018 and NUIG1.1-2021 employ rate parametrization adopted from their results, whereas the Arrhenius curves in other mechanisms are usually running lower, except for GRI3.0-1999 and Konnov-2009.

In Fig. 11, the presented rate coefficients of the various mechanisms match well with each other and the available direct measurements for R21, R24 and R25. In panel R20 (reaction $CH_2(S) + H_2O = CH_3OH$), USC-II-2007 uses similar reaction rate constant with Konnov-2009, while the other mechanisms have lower rate coefficients if the temperature is above 715 K. In addition, CRECK-2014 and two SanDiego mechanisms do not contain R20. For reaction R22: $CH_2(S) + O_2 = CO + OH + H$, the used rate constants of most mechanisms vary within very small range ($\sim 2.90\times10^{13}$ cm^3 mol^{-1} s^{-1}), while the R22 rate constant of NUIG1.1–2021 is significantly lower ($\sim 1.18\times10^{12}$ cm^3 mol^{-1} s^{-1}). Moreover, FFCM-I-2016, Konnov-2017 and Glarborg-2018 do not contain this reaction. In the panel of R23 ($CH_3 + OH = CH_2(S) + H_2O$), the rate coefficient used in FFCM-I-2016 almost matches the available direct experimental data and theoretical results, while the other mechanisms used different rate parameters. For reaction R26 $CH_2O + H = HCO + H_2$ in temperature range 1180 K – 1680 K there is significant difference between the direct measurements of Choudhury and Lin [76] and the other available direct measurements. Konnov-2009 used rate coefficient close to the experimental data of Choudhury and Lin [76], while the rate coefficients in other mechanisms are near to the other measurements.

For reaction R27: $CH_3OH (+ M) = CH_3 + OH (+ M)$ (LP, M = N_2) the available direct measurements concentrate on high temperature conditions (> 1400 K), in which the rate coefficients of all mechanisms can match the experimental results accurately.

Most mechanisms do not contain the reaction R28 ($CH_3 + O = H_2 + CO + H$), while it was identified as one of the most important reactions by sensitivity analysis in Glarborg-2018. Only four mechanisms (GRI3.0-1999, FFCM-I-2016, Konnov-2017 and Glarborg-2018) include R28, and the used rate coefficients are close to each other.

The sensitivity analysis of Glarborg-2018 also identified reaction R29 ($CH_2O + H = CO + H_2 + H$), which is present in this and the NUIG1.1-2021 mechanisms. This reaction proceeds through H abstraction and subsequent HCO (formyl) radical decomposition [77], thus it is different form the collision activated $CH_2O + M = CO + H_2 + M$ dissociation step that is present in all mechanisms (including Glarborg-2018 and NUIG1.1-2021) and where H can also be a collision partner. Hashemi et al. [78] emphasized the importance of HCO prompt decomposition on reproducing burning velocity, as a fraction of the HCO radicals from the reaction $CH_2O + H = HCO + H_2$ dissociate promptly to H + CO, and accelerates the flame propagating due to radical branching. On the contrary, the reactions of HCO with H, OH, or O_2 decelerate flame speed since they terminate the radical chain, therefore the competition between the two channels of HCO are important for reproducing flame speed. However, R29 reaction is missing in these widely used mechanisms.

Together with other missing steps $CH_2 + O_2 = CO_2 + H + H$ (R15), $CH_2(S) + O_2 = CO + OH + H$ (R22), $CH_3 + O = H_2 + CO + H$ (R28), step R29 represent a special class of reactions, in which three product molecules are formed. This behavior is due to the formation of a highly excited (e.g. HCOOH in the case of R15 [79]) or a weakly bound intermediate (e.g. HCO radical in the case of R29 [77]), which undergoes prompt dissociation before collisional stabilization and thermalization could take place. The possible importance of non-equilibrium effects for HCO radical decomposition in flame chemistry has been recognized recently [80] and further studies are in progress to clarify the relevance of such

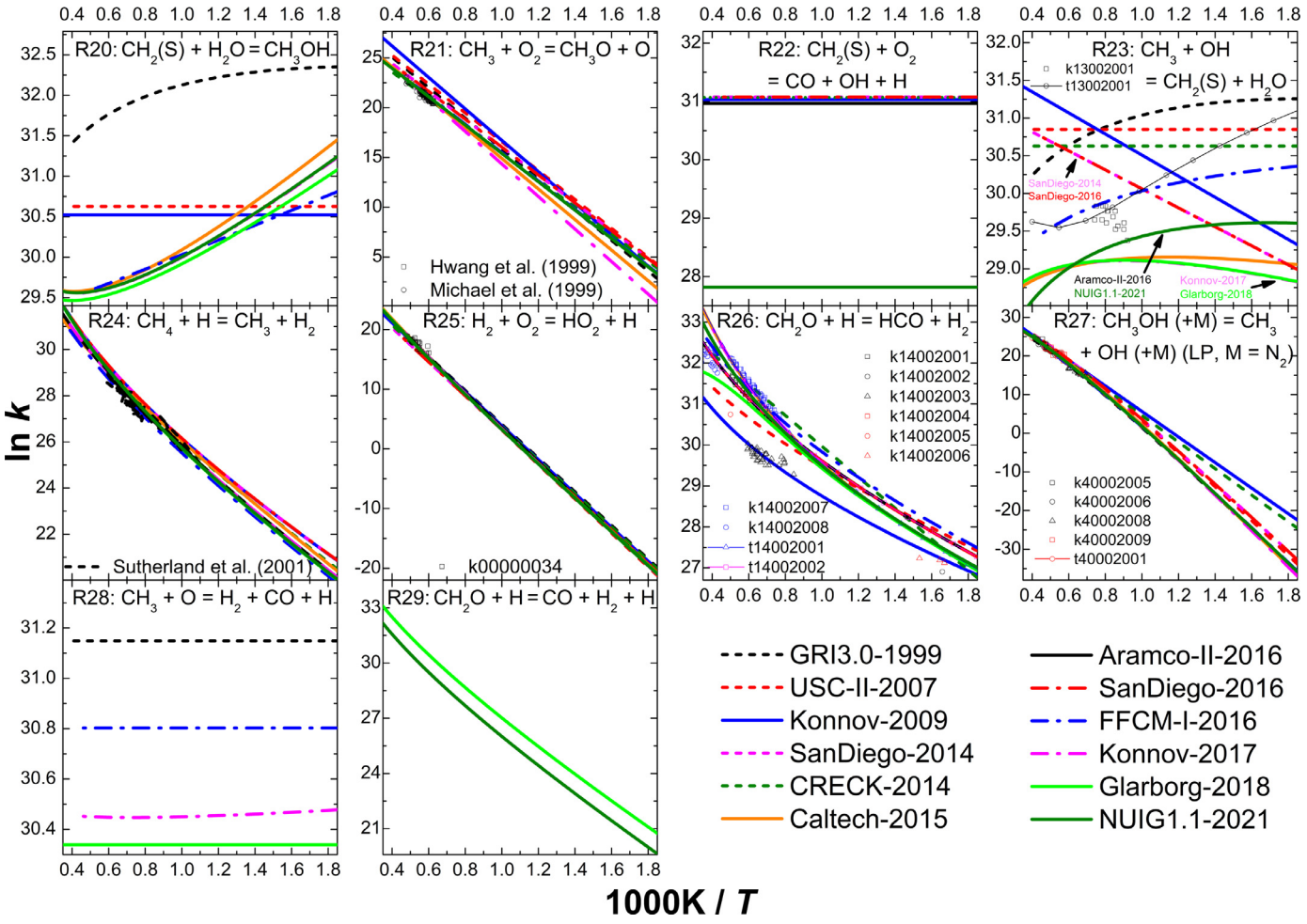

Fig. 11. Comparison of the rate parametrizations of important reactions R20 – R29 with the available direct determinations. The units of the rate coefficients are expressed in cm, mol, s. The ID numbers for the direct measurements are identical to the ReSpecTh database, the detailed reference is available in the Supplementary. More direct measurement data are used: Hwang et al. (1999) [73] and Michael et al. (1999) [74] for R21, Sutherland et al. (2001) [75] for R24. Scatter points: experimental direct determination of the rate coefficients, thin solid line with points: theoretical direct determination of the rate coefficients.

reactions of weakly-bound radicals to combustion chemistry (see e.g. [81]).

6.5. Effect of adding reaction steps to selected mechanisms

Table 3 shows that almost all of the most sensitive 29 reactions are present in the most accurate mechanisms. The exceptions are that reactions R28 and R29 are missing in Aramco-II-2016 and Konnov-2009, and R22 is missing in Glarborg-2018. After these three mechanisms, the other three good mechanisms are Caltech-2015, FFCM-I-2016, and NUIG1.1-2021. Reactions R15, R28 and R29 are not present in Caltech-2015, reactions R22 and R29 are missing in FFCM-I-2016, and R28 is not included in NUIG1.1-2021.

A series of extended mechanisms were created by adding separately each missing reaction step to the original mechanisms, and by adding all of them together. The details of these extensions are shown in Table 4. It has to be emphasized that complex reaction mechanisms are usually created in such a way that the parameters are assigned so that the whole obtained mechanism well describes all considered indirect measurement data. This means that even if the presence of another reaction step is chemically justified, it may spoil the general performance of a mechanism.

Figure 12 shows the performance of the modified mechanisms in reproducing the methane LBV measurements. Some modified mechanisms could not be simulated at the reproduction of some LBV measurements. To make the error function values E comparable for all investigated mechanisms, this figure is based on a reduced set of experimental data comprising 3458 data points in 345 datasets. Panel (a) shows that adding reaction R28 $CH_3 + O = H_2 + CO + H$ improved the performance of Aramco-II-2016 for measurements without helium, while it did not happen for adding R29 and the helium-containing measurements. Panel (b) demonstrates that adding reaction R28 slightly improves the performance of the Konnov-2009 mechanism, but adding R29 has a negative effect. The performance of the Glarborg-2018 mechanism was slightly improved for the helium-free measurements by adding reaction R22: $CH_2(S) + O_2 = CO + OH + H$ (see panel (c)). Adding reactions R15, R28 and R29 separately decreases the error of the Caltech-2015 mechanism, but adding all these steps results in higher error. Adding reactions R22 and R29 one by one significantly decreases the error of FFCM-I-2016 in reproducing methane-LBV measurements without helium, but adding both results in a more limited improvement. Also, adding R22 and/or R29 decreased the performance of FFCM-I-2016 in reproducing the measurements with helium. Panel (f) shows that the addition of R28 slightly improved the performance of NUIG1.1-2021 for the LBV measurements without helium, while it ill influenced the mechanism on the reproduction of helium-containing measurements.

The last three rows of Table 2 compare the performance of extended mechanisms Konnov-2009 + R28 (K + R28), Caltech-

Table 4
IDs of the extended mechanisms.

Mechanism IDs	Modifications in the mechanisms
Aramco-II-2016	The original mechanism without modification
A + R28	R28 of Glarborg-2018 was added to Aramco-II-2016
A + R29	R29 of Glarborg-2018 was added to Aramco-II-2016
A + R28+R29	R28 and R29 of Glarborg-2018 was added to Aramco-II-2016
Konnov-2009	The original mechanism without modification
K + R28	R28 of Glarborg-2018 was added to Konnov-2009
K + R29	R29 of Glarborg-2018 was added to Konnov-2009
K + R28+R29	R28 and R29 of Glarborg-2018 was added to Konnov-2009
Glarborg-2018	The original mechanism without modification
G + R22	R22 of Konnov-2009 was added to Glarborg-2018
Caltech-2015	The original mechanism without modification
C + R15	R15 of Glarborg-2018 was added to Caltech-2015
C + R28	R28 of Glarborg-2018 was added to Caltech-2015
C + R29	R29 of Glarborg-2018 was added to Caltech-2015
C + R15+R28+R29	R15, R28 and R29 of Glarborg-2018 were added to Caltech-2015
FFCM-I-2016	The original mechanism without modification
F + R22	R22 with the Konnov-2009 parameters was added to FFCM-I-2016
F + R29	R29 with the Glarborg-2018 parameters was added to FFCM-I-2016
F + R22+R29	R22 with the Konnov-2009 parameters and R29 with the Glarborg-2018 parameters were added to FFCM-I-2016
NUIG1.1–2021	The original mechanism without modification
N + R28	R28 of Glarborg-2018 was added to NUIG1.1–2021

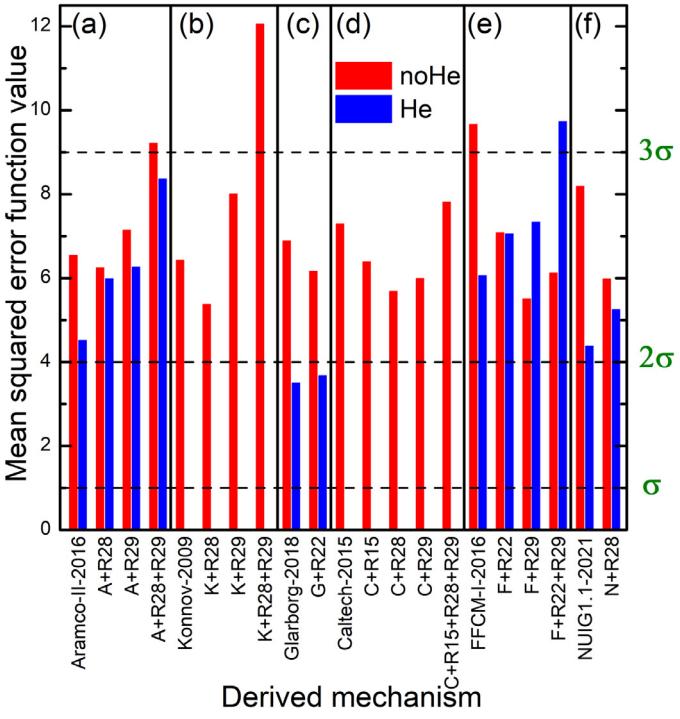

Fig. 12. Mean squared errors of the newly generated mechanisms (see Table 4) regarding the selected measurements (3270 data points in 336 datasets for helium-free measurements and 188 data points in 9 datasets are for helium- including measurements.).

2015 + R28 (C + R28) and FFCM-I-2016 + R29 (F + R29) on the whole set of data (4523 data points in 519 datasets) with all other mechanisms. Adding these reaction steps to the original mechanisms always improved the performance not only for all datapoints together, but in most cases in each measurement category (see the numbers in bold print). Considering also the extended mechanisms, the new order of performance is F + R29, C + R28, Aramco-II-2016, K + R28, Konnov-2009, and Caltech-2015 for all measurements without helium bath gas. Considering the helium containing measurements, mechanisms K + R28 and C + R28 are not applicable and the performance of extended mechanism F + R29 is not better than those of the original one.

7. Conclusions

Large amount of laminar burning velocity (LBV) experimental data of methane – oxygen – diluent mixtures (5500 data points in 646 datasets) measured using six different methods were collected from 111 publications. The fuel included pure methane or mixtures of methane with hydrogen and CO, but not other hydrocarbons or oxygenates. The diluents included nitrogen, H_2O, CO_2, Ar and He. The experimental techniques were the counterflow twin-flame method (CTF), single jet flame method (SJF), flame cone method (FCM), heat flux method (HFM), outwardly propagating flame method (OPF) and externally heated diverging channel method (HDC). The distribution of the collected LBV data as a function of cold side temperature, pressure, equivalence ratio and diluent ratio was investigated. All the experimental data files were encoded in RKD 2.3 format and the related details are available in the database of the ReSpecTh Information System [18].

We evaluated and compared the performance of 12 widely used methane combustion mechanisms published in the last two decades regarding their accuracy in simulating the collected experimental data in various regions of cold side temperatures, pressures, equivalence ratios and diluent ratios. The results show that most mechanisms could well predict the experimental LBVs for stoichiometric and fuel-lean mixtures and for mixtures with diluent ratios higher than 70%. Aramco-II-2016, Konnov-2009, Caltech-2015, Glarborg-2018, and NUIG1.1-2021 were the best performing mechanisms (in this order) at the reproduction of measurements without helium. Glarborg-2018 was the most accurate for helium containing LBV measurements. In our previous study of methane ignition delay times [1], Aramco-II-2016, Caltech-2015, Glarborg-2018 and SanDiego-2014 proved to be the best mechanisms. This means that the Aramco-II-2016, Glarborg-2018, and Caltech-2015 mechanisms have satisfactory performance for both the ignition delay time and laminar burning velocity measurements of methane ($+H_2$/CO)−oxygen−diluent mixtures. The Pearson correlation coefficients of the simulation results indicated that mechanisms within the two following sets: USC-II-2007 / SanDiego-2014 / SanDiego-2016 and Konnov-2009 / Caltech-2015 / Aramco-II-2016 / FFCM-I-2016 / Konnov-2017 / Glarborg-2018 / NUIG1.1-2021 are intrinsically similar as their signed simulation errors show high correlations considering the measurements without helium. These groupings reveal which previous mechanisms were used as a starting model at the development of later mechanisms. For the LBV mea-

surements with helium, the correlations of the simulation results are much weaker. The highest correlation coefficients are within mechanism sets USC-II-2007 / Aramco-II-2016 / SanDiego-2016 / Konnov-2017 / Glarborg-2018 and FFCM-I-2016 / NUIG1.1-2021.

The performance of the mechanisms was investigated at the conditions of compressed fresh mixture in the cylinders of natural gas engines using the data of Wang et al. [17]. We confirmed the statement of Wang et al. that these experimental data are well reproducible using mechanism FFCM-I-2016, and found that SanDiego-2014 and NUIG1.1-2021 perform similarly well. The simulation results obtained with SanDiego-2016, Aramco-II-2016 and Konnov-2017 are also within the 2σ error limits.

Local sensitivity analysis carried out at 18 typical cold side conditions (T: 300 / 400 K, p: 0.2 / 1 / 60 atm, φ: 0.5 / 1.0 / 2.0) using mechanisms Aramco-II-2016, Konnov-2009 and Glarborg-2018 identified 29 important reaction steps. For each of these 29 elementary reactions, the temperature dependence of the rate coefficient was shown on Arrhenius-type plots. These figures contained the rate coefficients as used in the 12 mechanisms (provided the reaction steps were included) and also selected direct measurements of the rate coefficients. By comparing rate coefficients among the mechanisms, it was found that the used rate coefficients in the mechanisms have obvious discrepancy with not only each other, but sometimes also with the available direct measurements.

The 29 reactions above are important in the three top mechanisms, but some of them are missing from several other mechanisms. We investigated the effect of adding the missing ones to the top 6 best-performing mechanisms. Considerably improvements were found by adding reactions R28 ($CH_3 + O = H_2 + CO + H$) to Konnov-2009, R28 to Caltech-2015 and R29 ($CH_2O + H = CO + H_2 + H$) to FFCM-I-2016.

Associated content

The following files are available free of charge.

List for the details of all collected experimental data collected in this study, supplementary figures and tables for sensitivity analysis result. (ch4_mech_comp_lbv_supp1. docx)

Estimated standard deviation for each experimental data point (ch4_mech_comp_lbv_supp2.txt)

Further data are available at the following web sites: (1) Laminar burning velocity experimental data at the ReSpecTh Information Site [18] (http://respecth.chem.elte.hu/respecth/reac/dofile.php?file=newZip/methane_LBV_v2_3.zip); (2) Rate parameters of the important reactions as used in the models, the related direct measurements and theoretical results are available in the *k-evaluation* web site [53].

Author contributions

The manuscript was written through contributions of all authors. All authors have given approval to the final version of the manuscript.

Funding sources

The authors acknowledge the financial support of the Hungarian National Research, Development and Innovation Office via NKFIH grants OTKA KH126515, K132109 and FK134332. The research within project No. VEKOP-2.3.2-16-2017-00013 was supported by the European Union and the State of Hungary, co-financed by the European Regional Development Fund. Mr. Peng Zhang was sponsored by China Scholarship Council.

Declaration of Competing Interest

The authors declare that they have no known competing financial interests or personal relationships that could have appeared to influence the work reported in this paper.

Supplementary materials

Supplementary material associated with this article can be found, in the online version, at doi:10.1016/j.combustflame.2021.111867.

References

[1] P. Zhang, I.G. Zsély, V. Samu, T. Nagy, T. Turányi, Comparison of methane combustion mechanisms using shock tube and rapid compression machine ignition delay time measurements, Energy Fuels 35 (2021) 12329–12351.
[2] A.A. Konnov, A. Mohammad, V.R. Kishore, N. Il Kim, C. Prathap, S. Kumar, A comprehensive review of measurements and data analysis of laminar burning velocities for various fuel+air mixtures, Prog. Energy Combust. Sci. 68 (2018) 197–267.
[3] Mechanical and aerospace engineering (combustion research) university of California at San Diego, chemical-kinetic mechanisms for combustion applications, San Diego Mechanism, 2016 https://web.eng.ucsd.edu/mae/groups/combustion/mechanism.html.
[4] H. Wang, X. You, A.V. Joshi, S.G. Davis, A. Laskin, F. Egolfopoulos, C.K. Law, USC Mech Version II. High-temperature combustion reaction model of H2/CO/C1-C4 compounds, 2007, (http://ignis.usc.edu/USC_Mech_II.htm).
[5] G.P. Smith, D.M. Golden, M. Frenklach, N.W. Moriarty, B. Eiteneer, M. Goldenberg, C.T. Bowman, R.K. Hanson, S. Song, W.C. Gardiner Jr, V.V. Lissianski, Z. Qin, GRI-Mech 3.0, 1999, (http://www.me.berkeley.edu/gri_mech/).
[6] A.A. Konnov, Implementation of the NCN pathway of prompt-NO formation in the detailed reaction mechanism, Combust. Flame 156 (2009) 2093–2105.
[7] A.N. Mazas, B. Fiorina, D.A. Lacoste, T. Schuller, Effects of water vapor addition on the laminar burning velocity of oxygen-enriched methane flames, Combust. Flame 158 (2011) 2428–2440.
[8] T. Le Cong, P. Dagaut, Effect of water vapor on the kinetics of combustion of hydrogen and natural gas: experimental and detailed modeling study, ASME Turbo Expo 2008: Power for Land, Sea, and Air (2008) 319–328, doi:10.1115/GT2008-50272.
[9] R.J. Varghese, H. Kolekar, V.R. Kishore, S. Kumar, Measurement of laminar burning velocities of methane-air mixtures simultaneously at elevated pressures and elevated temperatures, Fuel 257 (2019) 116120.
[10] NUI Galway Combustion Chemistry Centre, AramcoMech 2.0, 2017, (http://www.nuigalway.ie/combustionchemistrycentre/mechanismdownloads/aramcomech20/).
[11] G.P. Smith, Y. Tao, H. Wang, Foundational fuel chemistry model Version 1.0, 2016, (https://web.stanford.edu/group/haiwanglab/FFCM1/pages/FFCM1.html).
[12] S. Wang, Z. Wang, Y. He, X. Han, Z. Sun, Y. Zhu, M. Costa, Laminar burning velocities of $CH_4/O_2/N_2$ and oxygen-enriched $CH_4/O_2/CO_2$ flames at elevated pressures measured using the heat flux method, Fuel 259 (2020) 116152.
[13] X. Shen, X. Yang, J. Santner, J. Sun, Y. Ju, Experimental and kinetic studies of acetylene flames at elevated pressures, Proc. Combust. Inst. 35 (2015) 721–728.
[14] H. Zhao, J. Fu, F.M. Haas, Y. Ju, Effect of prompt dissociation of formyl radical on 1,3,5-trioxane and CH_2O laminar flame speeds with CO_2 dilution at elevated pressure, Combust. Flame 183 (2017) 253–260.
[15] E.J.K. Nilsson, A. van Sprang, J. Larfeldt, A.A. Konnov, Effect of natural gas composition on the laminar burning velocities at elevated temperatures, Fuel 253 (2019) 904–909.
[16] G. Capriolo, V.A. Alekseev, A.A. Konnov, An experimental and kinetic study of propanal oxidation, Combust. Flame 197 (2018) 11–21.
[17] Y. Wang, A. Movaghar, Z. Wang, Z. Liu, W. Sun, F.N. Egolfopoulos, Z. Chen, Laminar flame speeds of methane/air mixtures at engine conditions: performance of different kinetic models and power-law correlations, Combust. Flame 218 (2020) 101–108.
[18] ReSpecTh Information System, (http://respecth.hu/).
[19] T. Varga, C. Olm, P. Máté, B. Ágota, I. G. Zsély, ReSpecTh Kinetics Data Format Specification v2.3, (2020) available at: www.respecth.hu.
[20] T. Turányi, T. Nagy, I.G. Zsély, M. Cserháti, T. Varga, B.T. Szabó, I. Sedyó, P.T. Kiss, A. Zempléni, H.J. Curran, Determination of rate parameters based on both direct and indirect measurements, Int. J. Chem. Kinet. 44 (2012) 284–302.
[21] C. Olm, I.G. Zsély, R. Pálvölgyi, T. Varga, T. Nagy, H.J. Curran, T. Turányi, Comparison of the performance of several recent hydrogen combustion mechanisms, Combust. Flame 161 (2014) 2219–2234.
[22] C. Olm, I.G. Zsély, T. Varga, H.J. Curran, T. Turányi, Comparison of the performance of several recent syngas combustion mechanisms, Combust. Flame 162 (2015) 1793–1812.
[23] C. Olm, T. Varga, É. Valkó, H.J. Curran, T. Turányi, Uncertainty quantification of a newly optimized methanol and formaldehyde combustion mechanism, Combust. Flame 186 (2017) 45–64.

[24] C. Olm, T. Varga, É. Valkó, S. Hartl, C. Hasse, T. Turányi, Development of an ethanol combustion mechanism based on a hierarchical optimization approach, Int. J. Chem. Kinet. 48 (2016) 423–441.
[25] L. Kawka, G. Juhász, M. Papp, T. Nagy, I. Gy. Zsély, T. Turányi, Comparison of detailed reaction mechanisms for homogeneous ammonia combustion, Z. Phys. Chem. 234 (2020) 1329–1357.
[26] T. Nagy, Minimal Spline Fit - Model-free least squares fitting with Akima Splines, available from: *respect.hu*.
[27] T. Nagy, T. Turányi, Minimal Spline Fit: a model-free method for determining statistical noise of experimental data series, Proceedings of the European Combustion Meeting (2021) Paper 336.
[28] F.N. Egolfopoulos, P. Cho, C.K. Law, Laminar flame speeds of methane-air mixtures under reduced and elevated pressures, Combust. Flame 76 (1989) 375–391.
[29] C.K. Wu, C.K. Law, On the determination of laminar flame speeds from stretched flames, Symp. Int. Combust. 20 (1984) 1941–1949.
[30] C.M. Vagelopoulos, F.N. Egolfopoulos, Direct experimental determination of laminar flame speeds, Symp. Int. Combust. 27 (1998) 513–519.
[31] T.G. Scholte, P.B. Vaags, The burning velocity of hydrogen-air mixtures and mixtures of some hydrocarbons with air, Combust. Flame 3 (1959) 495–501.
[32] A. Van Maaren, L.P.H. De Goey, Stretch and the adiabatic burning velocity of methane- and propane-air flames, Combust. Sci. Technol. 102 (1994) 309–314.
[33] B. Lewis, G. von Elbe, Determination of the speed of flames and the temperature distribution in a spherical bomb from time-pressure explosion records, J. Chem. Phys. 2 (1934) 283–290.
[34] A.P. Kelley, C.K. Law, Nonlinear effects in the extraction of laminar flame speeds from expanding spherical flames, Combust. Flame 156 (2009) 1844–1851.
[35] M. Akram, S. Kumar, Experimental studies on dynamics of methane-air premixed flame in meso-scale diverging channels, Combust. Flame 158 (2011) 915–924.
[36] F.N. Egolfopoulos, N. Hansen, Y. Ju, K. Kohse-Höinghaus, C.K. Law, F. Qi, Advances and challenges in laminar flame experiments and implications for combustion chemistry, Prog. Energy Combust. Sci. 43 (2014) 36–67.
[37] Mechanical and Aerospace Engineering (Combustion Research) University of California at San Diego, Chemical-kinetic mechanisms For Combustion Applications, San Diego Mechanism, 2014 https://web.eng.ucsd.edu/mae/groups/combustion/mechanism.html.
[38] CRECK modeling Group C1-C3 kinetic mechanism Version 1412, 2014, (http://creckmodeling.chem.polimi.it/index.php).
[39] The FORCE - California Institute of Technology, CaltechMech detailed kinetic model (version 2.3), 2015, (https://www.theforce.caltech.edu/CaltechMech/).
[40] M. Christensen, A.A. Konnov, Laminar burning velocity of diacetyl + air flames. Further assessment of combustion chemistry of ketene, Combust. Flame 178 (2017) 97–110.
[41] P. Glarborg, J.A. Miller, B. Ruscic, S.J. Klippenstein, Modeling nitrogen chemistry in combustion, Prog. Energy Combust. Sci. 67 (2018) 31–68.
[42] Y. Wu, S. Panigrahy, A.B. Sahu, C. Bariki, J. Beeckmann, J. Liang, A.A.E. Mohamed, S. Dong, C. Tang, H. Pitsch, Z. Huang, H.J. Curran, Understanding the antagonistic effect of methanol as a component in surrogate fuel models: a case study of methanol/n-heptane mixtures, Combust. Flame 226 (2021) 229–242.
[43] Y. Yi, Personal communication. 2020.
[44] M. Frenklach, A. Packard, P. Seiler, R. Feeley, Collaborative data processing in developing predictive models of complex reaction systems, Int. J. Chem. Kinet. 36 (2004) 57–66.
[45] M. Papp, T. Varga, Á. Busai, I.G. Zsély, T. Nagy, T. Turányi, Optima++ package v2.1.0: a general C++ framework for performing combustion simulations and mechanism optimization. 2021.
[46] A. Cuoci, A. Frassoldati, T. Faravelli, E. Ranzi, OpenSMOKE++: an object-oriented framework for the numerical modeling of reactive systems with detailed kinetic mechanisms, Comput. Phys. Commun. 192 (2015) 237–264.
[47] OpenSMOKE++, (https://www.opensmokepp.polimi.it/).
[48] H. Pitsch, FlameMaster v4.0 BETA: a C++ computer program for 0D combustion and 1D laminar flame calculations. 2016.
[49] T. Turányi, A.S. Tomlin, Analysis of kinetic reaction mechanisms, Springer, 2014.
[50] BP statistical review of world energy 2020 (69th Edition); 2020.
[51] H. Niklas, White paper - Combustion engine power plants https://www.wartsila.com/docs/default-source/power-plants-documents/downloads/white-papers/general/wartsila-bwp-combustion-engine-power-plants.pdf.
[52] A. D'Adamo, M. Del Pecchia, S. Breda, F. Berni, S. Fontanesi, J. Prager, Chemistry-based laminar flame speed correlations for a wide range of engine conditions for iso-octane, n-heptane, toluene and gasoline surrogate fuels, SAE Int. (2017), doi:10.4271/2017-01-2190.
[53] Evaluation of high-temperature gas phase rate coefficients of elementary reactions https://k-evaluation.elte.hu/.
[54] T. Nagy, É. Valkó, I. Sedyó, I.G. Zsély, M.J. Pilling, T. Turányi, Uncertainty of the rate parameters of several important elementary reactions of the H2 and syngas combustion systems, Combust. Flame 162 (2015) 2059–2076.
[55] T. Varga, T. Nagy, C. Olm, I.G. Zsély, R. Pálvölgyi, É. Valkó, G. Vincze, M. Cserháti, H.J. Curran, T. Turányi, Optimization of a hydrogen combustion mechanism using both direct and indirect measurements, Proc. Combust. Inst. 35 (2015) 589–596.
[56] T. Varga, C. Olm, T. Nagy, I.G. Zsély, É. Valkó, R. Pálvölgyi, H.J. Curran, T. Turányi, Development of a joint hydrogen and syngas combustion mechanism based on an optimization approach, Int. J. Chem. Kinet. 48 (2016) 407–422.
[57] A.W. Jasper, S.J. Klippenstein, L.B. Harding, Theoretical rate coefficients for the reaction of methyl radical with hydroperoxyl radical and for methylhydroperoxide decomposition, Proc. Combust. Inst. 32 (2009) 279–286.
[58] Z.K. Hong, S.S. Vasu, D.F. Davidson, R.K. Hanson, Experimental study of the rate of OH + HO_2 = H_2O + O_2 at high temperatures using the reverse reaction, J. Phys. Chem. A 114 (2010) 5520–5525.
[59] Z. Hong, D.F. Davidson, K.-Y. Lam, R.K. Hanson, A shock tube study of the rate constants of HO_2 and CH_3 reactions, Combust. Flame 159 (2012) 3007–3013.
[60] A. Bonard, V. Daële, J.-L. Delfau, C. Vovelle, Kinetics of OH radical reactions with methane in the temperature range 295−660K and with dimethyl ether and methyl-tert-butyl ether in the temperature range 295−618K, J. Phys. Chem. A 106 (2002) 4384–4389.
[61] N.K. Srinivasan, M.-C. Su, J.W. Sutherland, J.V. Michael, Reflected shock tube studies of high-temperature rate constants for OH + CH_4 –> CH_3 + H_2O and CH_3 + NO_2 –> CH_3O + NO, J. Phys. Chem. A 109 (2005) 1857–1863.
[62] J.F. Bott, N. Cohen, A shock tube study of the reaction of the hydroxyl radical with H_2, CH_4, c-C_5H_{10}, and i-C_4H_{10}, Int. J. Chem. Kinet. 21 (1989) 485–498.
[63] N. Faßheber, G. Friedrichs, P. Marshall, P. Glarborg, Glyoxal oxidation mechanism: implications for the reactions HCO + O_2 and OCHCHO + HO_2, J. Phys. Chem. A 119 (2015) 7305–7315.
[64] S.-.O. Ryu, K.S. Shin, S.M. Hwang, Determination of the rate coefficients of the CH_4 + O_2 → HO_2 + CH_3 and HCO + O_2 → HO_2 + CO reactions at high temperatures, Bull. Korean Chem. Soc. 38 (2017) 228–236.
[65] R.S. Timonen, E. Ratajczak, D. Gutman, Kinetics of the reactions of the formyl radical with oxygen, nitrogen dioxide, chlorine, and bromine, J. Phys. Chem. 92 (1988) 651–655.
[66] M. Colberg, G. Friedrichs, Room temperature and shock tube study of the reaction HCO+O_2 using the photolysis of glyoxal as an efficient HCO source, J. Phys. Chem. A 110 (2006) 160–170.
[67] N.K. Srinivasan, M.-.C. Su, J.V. Michael, CH_3 + O_2 → H_2CO + OH Revisited, J. Phys. Chem. A 111 (2007) 11589–11591.
[68] N.K. Srinivasan, M.C. Su, J.W. Sutherland, J.V. Michael, Reflected Shock tube studies of high-temperature rate constants for CH_3 + O_2, H_2CO + O_2, and OH + O_2, J. Phys. Chem. A 109 (2005) 7902–7914.
[69] K. Saito, R. Ito, T. Kakumoto, A. Imamura, The initial process of the oxidation of the methyl radical in reflected shock waves, J. Phys. Chem. 90 (1986) 1422–1427.
[70] D.F. Davidson, M.D. Di Rosa, R.K. Hanson, C.T. Bowman, A study of ethane decomposition in a shock tube using laser absorption of CH_3, Int. J. Chem. Kinet. 25 (1993) 969–982.
[71] I.R. Slagle, D. Sarzynski, D. Gutman, Kinetics of the reaction between methyl radicals and oxygen atoms between 294 and 900K, J. Phys. Chem. 91 (1987) 4375–4379.
[72] J. Troe, V.G. Ushakov, The dissociation/recombination reaction CH_4 (+M) –>CH_3+H (+M): a case study for unimolecular rate theory, J. Chem. Phys. 136 (2012) 214309.
[73] S.M. Hwang, S.-.O. Ryu, K.J. De Witt, M.J. Rabinowitz, Rate coefficient measurements of the reaction CH_3 + O_2 = CH_3O + O, J. Phys. Chem. A 103 (1999) 5949–5958.
[74] J.V. Michael, S.S. Kumaran, M.-.C. Su, Rate constants for CH_3 + O_2 = CH_3O + O at high temperature and evidence for H_2CO + O_2 = HCO + HO_2, J. Phys. Chem. A 103 (1999) 5942–5948.
[75] J.W. Sutherland, M.C. Su, J.V. Michael, Rate constants for H + CH_4 , CH_3 + H_2 , and CH_4 dissociation at high temperature, Int. J. Chem. Kinet. 33 (2001) 669–684.
[76] T.K. Choudhury, M.C. Lin, Pyrolysis of methyl nitrite and 1,3,5-trioxane mixtures in shock waves: kinetic modeling of the H + CH_2O reaction rate, Combust. Sci. Technol. 64 (1989) 19–28.
[77] N.J. Labbe, R. Sivaramakrishnan, C.F. Glodsmith, Y. Georgievskii, J.A. Miller, S.J. Klippenstien, Weakly bound free radicals in combustion: "Prompt" dissociation of formyl radicals and its effect on laminar flame speeds, J. Phys. Chem. Lett. 7 (2016) 85–89.
[78] H. Hashemi, J.M. Christensen, S. Gersen, H. Levinsky, S.J. Klippenstein, P. Glarborg, High-pressure oxidation of methane, Combust. Flame 172 (2016) 349–364.
[79] P.-.F. Lee, H. Matsui, W.-.Y. Chen, N.-.S. Wang, Production of H and O(^{3}P) atoms in the reaction of CH_2 with O_2, J. Phys. Chem. A 116 (2012) 9245–9254.
[80] N.J. Labbe, R. Sivaramakrishnan, C.F. Goldsmith, Y. Georgievskii, J.A. Miller, S.J. Klippenstein, Ramifications of including non-equilibrium effects for HCO in flame chemistry, Proc. Combust. Inst. 36 (2017) 525–532.
[81] A.D. Danilack, C.F. Goldsmith, A statistical model for the product energy distribution in reactions leading to prompt dissociation, Proc. Combust. Inst. 38 (2021) 507–514.